J Geodesy
DOI 10.1007/s00190-006-0088-y

ORIGINAL ARTICLE

Estimating the noise in space-geodetic positioning: the case of DORIS

K. Le Bail

Received: 28 November 2005 / Accepted: 15 July 2006

Abstract The noise spectrum in DORIS ground-station motion is investigated by means of the Allan variance method applied to the decomposition of the 3D signal into its principal components in the time domain. Sets of weekly position time-series from 1994 to 2005 derived by three IDS Analysis Centres (IGN-JPL, INASAN, and LEGOS-CLS) for 119 stations at 69 sites are considered. The observing satellites are SPOT-2, SPOT-3, SPOT-4, and SPOT-5, TOPEX/Poseidon, and ENVISAT. Annual and semi-annual perturbations, as well as the 117.3-day term associated with the TOPEX/Poseidon orbit, are found at most stations. Their amplitudes reach up to 19.3, 23.7, and 13.3 mm, respectively, for the three analysis centres (ACs). When corrected for these components and a linear drift, the time-series dominantly show white noise (WN) at the 10–45 mm level: the noise level is the highest in the East direction, probably in connection with the high orbit inclinations. The noise level is minimum for the high latitude stations, mostly and intensively observed by the SPOT satellites, and the determination of the noise type is unclear; longer observation spans would be needed to decide between interannual variations and flicker noise. The improvement in positioning due to the DORIS constellation extension from three to five satellites in 2002, and the network rejuvenation program initiated in 2000, results in a decrease of the noise level by a factor of 1.7 in a WN context, both before and after the changes. One example of the benefit of studying the signal in the time-eigenspace domain is the detection of anomalously large WN in the East direction for station HBKB (Hartebeesthoek, Africa) that masks the above-mentioned improvement. Studying the projection on the local frame of the second and third time-eigenspace components, a noise excess is detected in the North direction for some of the ACs. Station stability derived from our time-series analysis confirms, in general, the expected performance based on the careful technical review of the station components (antenna, pillar, etc.). The respective merits of our noise qualification method, based on direct time-series analysis in the time-eigenspace domain without any a priori statistical model, in comparison with other methods, such as the selection of a mixed-noise model by maximum likelihood estimation, are discussed.

Keywords DORIS · Station coordinates · Time-series analysis · Principal component analysis (in the time domain) · Noise characteristics · Allan variance · Residual noise

K. Le Bail
GEMINI, Observatoire de la Côte d'Azur,
avenue Nicolas Copernic,
06130 Grasse, France

K. Le Bail (✉)
Laboratoire de Recherche en Géodésie,
Institut Géographique National,
6-8 avenue Blaise Pascal,
Champs Sur Marne,
77455 Marne La Vallée, France
e-mail: lebail@ensg.ign.fr

1 Introduction

DORIS was initially devised for precise orbit determination (POD) for Earth observation and altimetry. It is also used for positioning, in particular in the framework of the International DORIS Service (IDS) (Tavernier et al. 2005, 2006). Three analysis centres (ACs) submitted complete solutions for the International Terrestrial

Journal: 190 MS: 88 CMS: GIVE CMS ☐ TYPESET ☐ DISK ☐ LE ☐ CP Disp.:2006/8/18 Pages: 25

Reference Frame ITRF2005: *Institut Géographique National*, French Geographical Institute – Jet Propulsion Laboratory (IGN-JPL); Institute of Astronomy Russian Academy of Sciences (INASAN); and *Laboratoire d'Etudes en Géophysique et Océanographie Spatiales*, Laboratory of Spatial Studies in Geophysics and Oceanography – *Collecte et Localisation par Satellite*, Satellites Collection and Location (LEGOS-CLS).

DORIS positioning solutions are available, among other forms, as time-series of coordinates at weekly intervals. Good quality results start in 1994, allowing a detailed investigation of the stability of station positions. Qualifying the DORIS station stability is particularly important in view of the IDS contribution to the International Earth Rotation and Reference Systems Service (IERS), in parallel to the three other geodetic services: IVS (http://www.ivscc.gsfc.nasa.gov; Schlueter et al. 2002) for VLBI, IGS (http://www.igscb.jpl.nasa.gov; Beutler et al. 1999) for GPS, and ILRS (http://www.ilrs.gsfc.nasa.gov; Pearlman et al. 2002) for laser ranging.

Advanced time-series analysis is a quite recent research field in space geodesy. Pioneering studies were undertaken in the late 1990s in the GPS domain by King et al. (1995), Langbein and Johnson (1997), and Zhang et al. (1997). These authors implement standard statistical tools, e.g. spectral density or maximum likelihood estimation (MLE), separately on the North, East, and Up components (NEU) of the time-series, in order to determine the noise composition of each component. Assuming that the noise spectrum in the considered time-series is a linear combination of white noise (WN), flicker noise (FN) and random walk noise (RWN), one writes the signal covariance matrix as a linear combination of these different models. The values of the linear combination coefficients ("variance components") are estimated by finding values that maximize the corresponding likelihood function (Langbein and Johnson 1997).

These studies generally conclude that the non-linear signal in GPS station motion can be described as a combination of WN and FN. Zhang et al. (1997), Mao et al. (1999), and Nikolaidis (2002) used MLE primarily to test models with FN + WN, RWN + WN and WN only. For models where they assumed a general spectral index, there was – at that time – no known way to produce a covariance matrix, so lines were fit to the power spectra. However, it was the MLE results that were the main thrust of the paper. Williams et al. (2004) used only MLE. The main focus of Williams (2003) was the empirical estimation of rate uncertainties. Zhang et al. (1997) first subtracted the regional common non-tectonic signals by use of a filtering algorithm. They concluded from the analysis of 1.6 years of GPS data that the time-series are characterized by a combination of WN and FN. Mao et al. (1999), Nikolaidis (2002), Williams (2003), and Williams et al. (2004) also find a combination of WN and FN.

We developed a statistical analysis tool to identify the noise level and noise spectrum of time-series of space-geodetic station coordinates (Le Bail 2004), which can also be used to compare the results of the different ACs. Our approach differs from this "classical" one in several aspects, as

1. it transforms the three-dimensional (3D) series of coordinates into its eigenspace in the time domain, which allows the separation of independent noise components. The original time-series in the NEU space may be correlated as a result of network configuration, observation rates, orbit passes, geometry, etc. In the DORIS and GPS cases, the correlations are small (Le Bail 2004), thanks to an overall balanced observational geometry. However, the projection onto the time-like eigenspace brings independent information of a new type,
2. it makes use of the Allan variance (Allan 1966, 1987; Rutman 1978; Azoubib 1974), a classical tool in time and frequency standard metrology, to characterize the type and level of noise without any a priori model assumption.

Section 2 presents the data analysed. They were derived for the global station network by three IDS ACs. Section 3 describes the statistical tools used, i.e. principal component analysis in the time domain (Sect. 3.1) and Allan variance statistics (Sect. 3.2). A detailed application to four DORIS stations and the respective co-located GPS stations is shown in Sect. 4. The spectral behaviour of the whole DORIS network is described in Sect. 5, in both the local NEU reference frame and the time-like eigenspace. Section 6 is dedicated to the investigation of the correlation of the spectrum and level of noise of the station positions with various instrumental, observational, and geographical characteristics.

2 Data

Time-series of DORIS station coordinates may be available under different forms as series of coordinates referred to ITRF2000 [STation Coordinates Difference (STCD)] and/or time-series of weekly free-network solutions as Software INdependent EXchange format (SINEX) files. Four IDS ACs provide this last type of time-series: IGN-JPL (version ignwd05; Willis and Heflin 2004), INASAN (version inawd03; Kuzin and Tatevian 2006), both using the GIPSY-OASIS II

Journal: 190 MS: 88 CMS: GIVE CMS ☐ TYPESET ☐ DISK ☐ LE ☐ CP Disp.:2006/8/18 Pages: 25

software package (Webb and Zumberge 1997), LEGOS-CLS (version lcawd12; Soudarin et al. 2002; Crétaux et al. 2002) using the GINS-DYNAMO software developed by the French *Groupe de Recherches de Géodésie Spatiale* (GRGS – Space Geodesy Research Group), and Goddard Space Flight Centre (GSFC) (gscwd02 version; Willis et al. 2005, in press) using GEODYN (Pavlis et al. 2000).

The present study is based on the first three solutions, spanning more than 10 years. The last one, covering only 1 year, a time span too short to derive robust spectral diagnoses, could not be used. Discontinuities are properly handled in the Combination and Analysis of Terrestrial Reference Frames (CATREF) software (Altamimi et al. 2002) processing. Residuals relative to a 3D linear motion without jump (for example, those pointed out by the ACs) are obtained. The STCD files are also available including IGN-JPL and LEGOS-CLS solutions. We do not use them because the LEGOS-CLS time-series are monthly and do not provide a sufficient number of measurement for statistical meaning. Furthermore, considering solutions that referred to ITRF2000 with the same method permits to check the DORIS noise consistency.

The DORIS oscillator onboard Jason-1 produces large anomalies in station positioning over the South Atlantic Anomaly (SAA) (Willis et al. 2004). Therefore, Jason-1 data are not used: the three ACs computed data from SPOT-2, SPOT-3, SPOT-4, SPOT-5, TOPEX/Poseidon, and ENVISAT. A correction model for the effect on Jason1 DORIS oscillator is now available, derived by Lemoine and Capdeville (2006). All groups used their own analysis strategy, implying differences in the models and processing strategies. These are documented at the IDS Data Centre (see, e.g., ftp://cddis.gsfc.nasa.gov/doris/ products/sinex_series/, files ending with '.dsc' in each directory) and Willis et al. (2005, in press) made some comparisons between three ACs' solutions including IGN-JPL and LEGOS-CLS ones to find some systematic error in DORIS scale.

In principle, these differences may be expected to produce systematic differences or different noise signatures. Among the systematic differences, a particular feature is the 117.3-day period for TOPEX/Poseidon, which is related to the period of the orbit plane toward the Sun: the node rate of the orbit with respect to the Sun is −3.0679°/day, taking exactly 117.3 days to go 360°. This error could be related to mismodelling error in the TOPEX/Poseidon concerning the solar pressure computation or estimation (P. Willis, personal communication). This period is seen in the time-series of station coordinates.

The time-series of free-network solutions, or loosely constrained solution in the case of LEGOS-CLS, were referred to ITRF2000 by J.-J. Valette using the CATREF software at the IDS Central Bureau (Tavernier et al. 2006). CATREF includes a projection (Sillard and Boucher 2001) and a seven-parameter transformation into ITRF2000. Breaks (mentioned in Table 1), local ties, and velocities in the same site are taken into account in the processing. The output data are under the form of weekly time-series of residuals and formal errors in local directions to the NEU frame. The time-series provided by IGN-JPL, INASAN, and LEGOS-CLS concern a total of 119 stations at 69 sites (Fig. 1). They are briefly described in Table 2.

The Allan variance analysis (see Sect. 3.2), used to estimate the noise level and spectrum of the station coordinates, requires time-series with equally spaced data. The less the data gaps need to be filled, the more robust the statistics are. The noise spectrum is determined on the basis of the Allan variance for increasing data sampling times. Obviously, longer time-series will allow a better spectrum estimation. Therefore, we classified the station time-series into three categories according to their length and density, reflecting the expected reliability of the derived statistics. The categories are as follows:

- C1: time-span longer than 3 years, less than 30% of missing weeks and data gaps shorter than 200 days;
- C2: same as above, with some data gaps longer than 200 days, but still shorter than 400 days;
- C3: the other stations, i.e. those with less than 3 years of data, or with gaps longer than 400 days.

A number of stations have a short data span because their ground-beacons were recently replaced in the framework of the network rejuvenation project. Stations for which an earthquake was identified (e.g. Arequipa and Fairbanks) are considered as category C3 because our filtering model does not include individual post-seismic relaxation processes (Willis and Ries 2005).

The data-gaps filling technique is as follows. An ad hoc model consisting of a bias, a linear drift, annual, semi-annual, and 117.3-day periodic components is removed from the time-series of CATREF residuals using least-squares. For a time-series with mean m and variance σ^2, missing data are reconstructed by adding back to the model synthetic noise following a normal law $\mathcal{N}(m, \sigma)$. Tests have shown that this method gives, for C1-category stations, the same results in terms of type of noise or distribution of the principal components, but it implies an increase of about 5% of the level of noise. In the case of long data gaps (C2 and C3 stations), it tends to slightly emphasize WN.

Journal: 190 MS: 88 CMS: GIVE CMS ☐ TYPESET ☐ DISK ☐ LE ☐ CP Disp.:2006/8/18 Pages: 25

Table 1 List of introduced breaks and specific information on stations

Station	Analysis centres	Date	Break or deletion	Comment
AREA/Arequipa	All the analysis centres	June 23, 2001	Break	Earthquake
AMSA/Amsterdam	IGN-JPL/INASAN	After Jan 1, 1996	Deletion	Antenna fall
AMSB/Amsterdam	IGN-JPL/INASAN	All	Deletion	Antenna fall
COLA/Colombo	All the analysis centres	Nov 1994	Break	
DIOA/Dyonisos	All the analysis centres	April 1, 1995	Break	
SAKA/Sakhalin	All the analysis centres	Oct 5, 1994	Break	Earthquake on Oct 4, 1994
		Dec 26, 1999	Break	
KRAB/Krasnoyarsk	All the analysis centres	Nov 1999	Break	
SODA/Soccorro Is.	IGN-JPL/INASAN	Before Jan 1, 1996	Deletion	Volcano depletion
SODB/Soccorro Is.	All the analysis centres	Oct 3, 2002	Break	Earthquake on Oct 3, 2002
OTTA/Ottawa	All the analysis centres	Apr 25, 1991–May 28, 1991	Deletion	Antenna fall
		May 29, 1991	Break	
		Sept 1, 1993–Jan 31, 1994	Deletion	Antenna fall
		Feb 1, 1994	Break	
		Jan 4, 1998–Jan 28, 1998	Deletion	Antenna fall

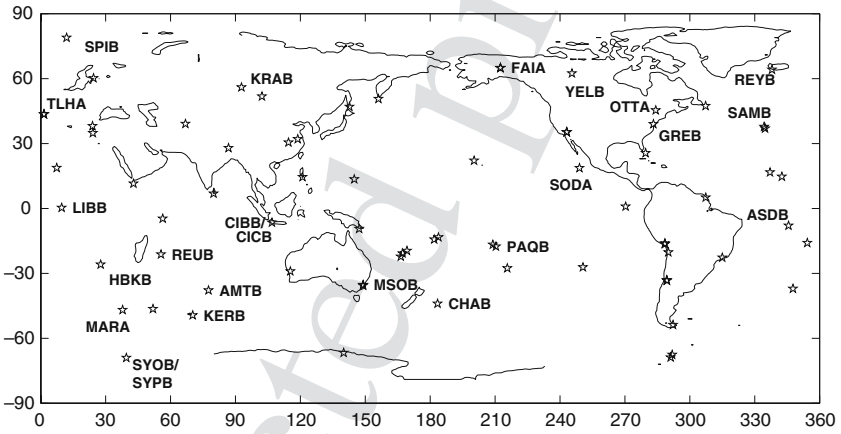

Fig. 1 DORIS sites analysed in this study (119 stations at 69 sites and four-character ID of the stations that are mentioned in the text) [Mercator projection]

Table 2 The sets of station coordinates analysed. C1, C2, and C3 correspond to the number of stations in these three criteria

DORIS series (version)	Data span	Stations	C1	C2	C3
IGN-JPL (ignwd05)	1994.1–2005.2	118	51	10	57
INASAN (inawd03)	1994.1–2004.4	110	52	9	49
LEGOS-CLS (lcawd12)	1994.1–2005.0	114	60	11	43

3 Analysis method

The analysis method proposed makes use of principal component analysis (PCA), a classical statistical tool implemented here in the time domain, coupled with the Allan variance, a classical tool in time and frequency metrology. It allows separation of independent noise contributions by decorrelating them temporally, and characterization of their spectra directly, as opposed to testing various mixed-noise models in parallel in the three NEU directions of the local frame.

3.1 PCA in the time domain

We analyse each station's time-series as the temporal evolution of a 3D vector, using PCA in the time domain (PCAT), derived from the standard PCA (Saporta 1978; Baccini and Besse 1999; Le Bail 2004).

We form the cross-covariance in time (and not in space) of the 3D time-series:

$$C(S,T) = \frac{1}{n}\sum_{i=1}^{n}(S(t_i)-\bar{S})(T(t_i)-\bar{T}) \quad (1)$$

where n is the number of observations in the time-series, t_i is the date i, S and T are, e.g., the time-series of N, E, or U residuals. $\bar{S} = \frac{1}{n}\sum_{i=1}^{n} S(t_i)$ is the average of the Svariable.

C is a 3×3 symmetric matrix containing the temporal variances and covariances between the (N, E, U) residuals. Note that this matrix, which is empirically estimated from the time behaviour of the data itself, is different from the usually considered geometrical variance/

Journal: 190 MS: 88 CMS: GIVE CMS ☐ TYPESET ☐ DISK ☐ LE ☐ CP Disp.:2006/8/18 Pages: 25

covariance (VCV) matrix that results from global network least-squares analysis.

The three initial time-series are then projected on the eigenspace of C with

$$(\mathrm{PC1}, \mathrm{PC2}, \mathrm{PC3}) = (\mathrm{d}N, \mathrm{d}E, \mathrm{d}U)V \tag{2}$$

where PCi is the coordinate of the ith component based on the ith projection, and V contains the eigenvector coordinates of C in its columns.

This space has, by definition, three temporally uncorrelated axes (since the matrix generating the space is diagonal), each of which explains a part of the initial signal that is quantified by the variance percentage:

$$\%\mathrm{Var}_i = \frac{\lambda_i}{\sum_{i=1}^{3} \lambda_i} \tag{3}$$

where λ_i is the$i$th eigenvalue of C.

C is a positive-definite matrix by definition (Papoulis and Pillai 2002): each of the three eigenvalues λ_i is non-negative. Therefore, $\%\mathrm{Var}_i$ is also non-negative.

This decomposition gives access to the hierarchy of components that explain the signal in the time domain for the data span considered. It reflects the time consistency of the 3D signal, independently of the space-like correlations that are induced by the geographical distribution of the network, data acquisition rates, and station-orbit configuration.

3.2 Allan variance analysis

To analyse the spectrum and the level of noise for each component, we use the Allan variance (Allan 1966, 1987; Rutman 1978; Azoubib 1974).

Let S be a time-series with constant time interval τ_0. The Allan variance is defined by

$$\sigma_S^2(\tau) = \langle (\bar{S}_{k+1} - \bar{S}_k)^2 \rangle \tag{4}$$

where $\bar{S}_k = \frac{\tau_0}{\tau} \sum_{i=l}^{l+\frac{\tau}{\tau_0}-1} S(t_i), l \in \{1, \ldots, +\infty\}$, τ is a variable sampling time, and $\langle \cdot \rangle$ denotes the average.

As we are in a finite case, we use an estimator of the Allan variance – the overlapping estimator (Greenhall 1991):

$$\hat{\sigma_S^2}(\tau) = \frac{1}{2(N - 2\frac{\tau}{\tau_0} + 1)} \sum_{i=l}^{N-2\frac{\tau}{\tau_0}+1} \left(\bar{S}_{k+\frac{\tau}{\tau_0}, \frac{\tau}{\tau_0}} - S_{k, \frac{\tau}{\tau_0}} \right)^2 \tag{5}$$

where $\bar{S}_{k+\frac{\tau}{\tau_0}, \frac{\tau}{\tau_0}} = \frac{\tau}{\tau_0} \sum_{i=l}^{l} S(t_i), l \in \left\{1, \ldots, N - \frac{\tau}{\tau_0} + 1\right\}$, N is the total number of points.

The studied time-series are residuals from least-squares analysis. By assumption, the distribution of the residuals is Gaussian or normal. Thus, considering a sample $Y = (Y_i)_i$ following a Gaussian law, $\sum_i Y_i^2$ follows a χ^2-law. A 90% confidence interval is then computed as (Howe et al. 1981)

$$\frac{\mathrm{dof} \times \hat{\sigma_S^2}}{\chi^2_{\mathrm{dof}}(0.90)} < \sigma_S^2 < \frac{\mathrm{dof} \times \hat{\sigma_S^2}}{\chi^2_{\mathrm{dof}}(0.10)} \tag{6}$$

where dof is the degree of freedom depending on the length of the sampling and of $\frac{\tau}{\tau_0}$, and $\chi^2_{\mathrm{dof}}(\cdot)$ is the appropriate χ^2-distribution.

The Allan variance can be expressed as a function of the power spectral density (PSD) (Allan 1987):

$$\sigma_S^2(\tau) = 2 \int_0^{+\infty} S_X(f) \frac{\sin^4(\pi f \tau)}{(\pi f \tau)^2} \mathrm{d}f \tag{7}$$

where $S_X(f) = P_0 f^{\alpha}$ is the PSD, α is the spectral index, P_0 is a constant, and f the frequency.

Processing the Allan variance analysis for $\tau = \tau_0, 2\tau_0, 4\tau_0, \ldots$, we plot the results on a log–log graph:

$$\log(\hat{\sigma_S^2}(\tau)) = \mu \log(\tau) \tag{8}$$

The slope μ and the spectral index α can be linked using Eq. (7). Then μ identifies the noise spectrum, with $\mu = -1$ for WN, $\mu = 0$ for FN, and $\mu = +1$ for RWN. White noise corresponds to a spectral density S independent of the frequency f, which means that each point of the time-series is independent of the others. Coloured noise like FN (S proportional to f^{-1}) or RWN (S proportional to f^{-2}) means that the points of the time-series are correlated (at a lower level for FN than for RWN), so that a point depends on the history of all the points.

The signature of a linear slope in the signal is $\mu = +2$. The signature of a periodic component in the signal in the Allan graph is a dip when τ is equal to the cycle period and a bump at about half of the cycle period, with a size that depends on the signal/noise ratio of the amplitude of the cyclic component (Le Bail 2004).

For a process composed of two independent noise components, the resulting Allan graphs shows the superimposition of both signatures, with relative levels reflecting their respective amplitudes. With this method, no a priori assumption on the type of noise is necessary: the type and level are read directly from the graph.

3.3 Application to time-series of geodetic station coordinates

The general tools described in Sects. 3.1 and 3.2 are now applied to time-series of space-geodetic station coordinates in the NEU frame. Le Bail (2004) showed that the method provides same results for the NEU coordinates than for the XYZ coordinates projected on the

Journal: 190 MS: 88 CMS: GIVE CMS ☐ TYPESET ☐ DISK ☐ LE ☐ CP Disp.:2006/8/18 Pages: 25

Table 3 Amplitudes of periodic signals in the DORIS residual time-series of station coordinates: annual and semi-annual terms, 117.3-day term for IGN-JPL, INASAN, and LEGOS-CLS DORIS analysis centres

Amplitudes in mm	Annual term average [max. min.]	Semi-annual term average [max. min.]	117.3-day term average [max. min.]
IJN-JPL			
North	6.8 [0.5 15.8]	3.2 [0.7 8.0]	5.0 [0.5 19.3]
East	4.1 [0.3 12.0]	3.3 [0.1 10.2]	4.3 [0.6 17.9]
Height	4.1 [0.3 12.0]	3.3 [0.3 7.3]	4.4 [0.2 14.2]
INASAN			
North	7.3 [0.2 19.8]	3.1 [0.4 7.0]	5.5 [0.4 23.7]
East	4.4 [0.9 12.0]	3.4 [0.1 10.3]	4.8 [0.7 14.2]
Height	4.4 [0.9 12.0]	3.1 [0.3 8.5]	4.6 [0.3 15.7]
LEGOS-CLS			
North	4.3 [0.0 16.5]	2.8 [0.0 14.0]	2.5 [0.0 13.3]
East	6.4 [0.0 17.9]	4.0 [0.1 15.2]	3.5 [0.0 12.0]
Height	6.4 [0.0 17.9]	3.1 [0.2 10.3]	2.9 [0.2 9.0]

NEU frame. Therefore, we choose here to study NEU coordinates to make easy the interpretations.

The dominant signal component in the time-series of station positions is usually modelled as a linear drift in the three components. The instability in the time-series is assumed to take place in the remaining part of the signal. It may be related to local geophysical phenomena, instrumentation, the analysis strategies, or insufficient modelling. Our study focusses on this part of the signal, i.e. residuals relative to a 3D linear motion model for each station individually. These residuals may contain seasonal signatures, in particular in the height component, or technique-specific periods such as the 117.3-day DORIS perturbation.

A summary of the size of these periodic terms is given in Table 3. The annual term has the largest amplitude, with an average of 4.3, 6.8, and 7.3 mm for the North component in the LEGOS-CLS, IGN-JPL, and INASAN solutions respectively, then the 117.3-day term with amplitudes from 4.3 to 5.0 mm for IGN-JPL, 4.6–5.5 mm for INASAN, and 2.5–3.5 mm for LEGOS-CLS. The semi-annual term shows amplitudes around 3.5 mm for the three ACs. The first harmonics of the annual term have smaller amplitudes than the 117.3-day term (Blewitt and Lavallée 2002), which is close to the second harmonics. This would be consistent with the expectation that the 117.3-day term has a non-seasonal origin.

These components play no role in the long-term station stability. On the other hand, their contribution to the Allan graph in the sub-annual band would mask an underlying WN signature (-1 slope), and the sum of the two signatures would then be wrongly interpreted as a FN signature (null slope). To avoid the latter difficulty without influencing the long-term stability diagnosis, the Allan graphs are derived from time-series corrected for the appropriate periodic terms.

The analysis method proceeds in several steps, as follows:

1. The initial time-series are corrected for a drift, a constant bias, and periodic terms (annual, semi-annual, 117.3-day, referred to as extended seasonal model hereafter) estimated by least-squares over the total data span.
2. PCAT is applied to these time-series, providing the three, PC1, PC2, PC3, components.
3. Data gaps are filled as described above.
4. Allan variance analysis is performed on each PC1, PC2, PC3 to determine its noise spectrum. This step can also apply to the series in the local N, E, U frame.
5. In addition to the value of the "Allan standard deviation" explained as the (positive) square-root of the Allan variance to quantify the quality of the residual coordinates, the spectrum is determined by the slope of the so-called Allan graph, where the Allan variance σ_S^2 is plotted as a function of the sampling time τ in log–log scale. The slope is estimated by weighted least-squares, and the probability for which the assumption of a linear drift is realistic is derived by a Fisher test. Values of the Fisher test probability higher than 0.8 are considered satisfactory.

Note that this method, by essence, does not allow one to account for internal errors, and – like in other time-series analysis methods – a fundamental assumption is the homogeneous quality of the data over the total data span. This implies various aspects of persistence, such as permanent quality of the monumentation or stability of the number of observations.

The history of the DORIS program is marked by the progressive extension of the satellite fleet and by the rejuvenation program of the stations (Fagard 2006), with improved quality monumentation and equipment starting to be installed in 2000. For this reason, the station stability analysis is performed separately for the different stations in each site.

Concerning the amount of observations, two satellites were collecting the ground-beacon signals in 1993 and in 1997, three over 1994–1996 and 1998.0–2002.4, and five over the period from 2002.4 until the end of the DORIS data on-board TOPEX/Poseidon in November 2004. As a result, the short term scatter of the weekly positioning solutions is decreased by a factor of 2 between 2000 and 2005 (Tavernier et al. 2006). For the stations with time-series overlapping these time periods, the estimated level describes an average situation. Only

Journal: 190 MS: 88 CMS: GIVE CMS ☐ TYPESET ☐ DISK ☐ LE ☐ CP Disp.:2006/8/18 Pages: 25

one-fourth of the station time-series are significantly affected by the change in data quality. A few well-observed stations could be used to evaluate the impact of the increased number of observations (Sect. 6.3). One should note, however, that our method describes the ability of the DORIS system to study long-term phenomena as provided by the existing time-series.

4 Testing the method on DORIS and GPS data

To help figure out the detailed structure of our results and various aspects of their interpretation, we show in Sect. 4.1 examples of results in the local N, E, U frame for three DORIS stations: Cibinong (CIBB, Indonesia), Chatham Island (CHAB, New-Zealand), and Kerguelen (KERB, France T.A.A.F.). The time-series analyses of these stations are further compared in Sect. 4.2 with those of the respective co-located GPS stations (BAKO, CHAT, KERG), using the time-series derived by the Centre for Orbit Determination in Europe (CODE) with the Bernese GPS software (Hugentobler et al. 2005, 2006). The comparison is made in the PC1, PC2, PC3 time-eigenspace.

As another illustration, we show (in Sect. 4.3) the example of the HBKB DORIS station in Hartebeesthoek (Africa), where the PCAT results provide evidence for the presence of an independent noise source in the East direction that would not be seen by the direct inspection of the series of residuals.

From here on, all time-series are under the form of residuals to the linear and extended seasonal models mentioned in Sect. 3.3. In addition, to avoid biasing the stability estimations by early results based on only two satellites, weekly solutions are considered only after 1994.1.

4.1 Spectral behaviour in the local frame: DORIS

The observation of the studied DORIS stations span 1994.1–2000.7 for CIBB, 1999.2–2005.2 for CHAB, and 1995.0–2001.2 for KERB. Figure 2 shows their Allan graphs in the N, E, U directions. Numerical results for the Allan graph slope and the 7-day "Allan standard deviation" are given in Table 4. For the three ACs, the Allan plots are very close to each other. They show quasi-identical properties of type and level of noise for all N, E, U components in the three stations.

The case of the North component of KERB is peculiar: the LEGOS-CLS curve is at a level comparable to those of the other stations, whereas the IGN-JPL and INASAN level of noise is larger, the difference reaching nearly half an order of magnitude for the 1-year sampling time. An important point to notice is that the IGN-JPL and the INASAN do not use the 1998 SPOT4 data contrary to the LEGOS-CLS. This could explain why the obtained level of noise is lower for the LEGOS-CLS KERB solution than for the two others ACs (P. Willis, personal communication). Willis et al. (2006) found an error in the DORIS SPOT4/1998 data preprocessing and proposed an easy way to incorporate these data in future solutions.

4.2 Spectral behaviour in the time-eigenspace domain: DORIS and GPS

The observations of the studied GPS stations span 1999.7–2005.7 for BAKO and 1996.1–2005.7 for CHAT and KERG. The overlapping DORIS-GPS periods cover 2 years at Cibinong, 6 years at Chatham Island, and 5 years at Kerguelen. The results of the analyses for the three pairs of DORIS and GPS stations are given in Table 5. PC1, PC2, and PC3 are the three principal components in the time domain, in order of decreasing percentage of explained variance (%Var).

As an example, for the Cibinong DORIS station in the IGN-JPL solution, the non-linear, non-seasonal signal can be decomposed into three independent signals, a 29–34 mm WN explaining 47% of the variance for $\tau = 7$ days, a 21–24 mm WN explaining 28% of the variance, and a 21–25 mm WN explaining 25% of the variance. For each PC_i and each AC, Table 5 gives the Allan graph slope and its interpretation in terms of type of noise and the "Allan standard deviation" for the 7-day sampling time in the form of the confidence interval. The type of noise comprises: white noise (Wh) for slopes close to -1, flicker noise (Fl) for slopes close to 0, and inconclusive noise type (In) where the formal uncertainty of the estimated slope does not allow one to decide between the -1 and 0 values.

The results for the three DORIS stations derived from the three ACs are close to each other for all listed parameters. The white noise signatures are clear, with the Allan graph slopes close to -1 for all three principal components. The type of noise of the GPS stations is clearly FN in the three cases.

The Allan graphs for each of the three DORIS and GPS stations are plotted in Fig. 3. The instability of the station coordinates is larger for DORIS than for GPS for the 7-day sampling time. However, as already mentioned by Le Bail et al. (2006), as a result of their respective white noise and flicker noise signatures, the stability of DORIS positioning converges towards that of GPS in the longer term.

Journal: 190 MS: 88 CMS: GIVE CMS ☐ TYPESET ☐ DISK ☐ LE ☐ CP Disp.:2006/8/18 Pages: 25

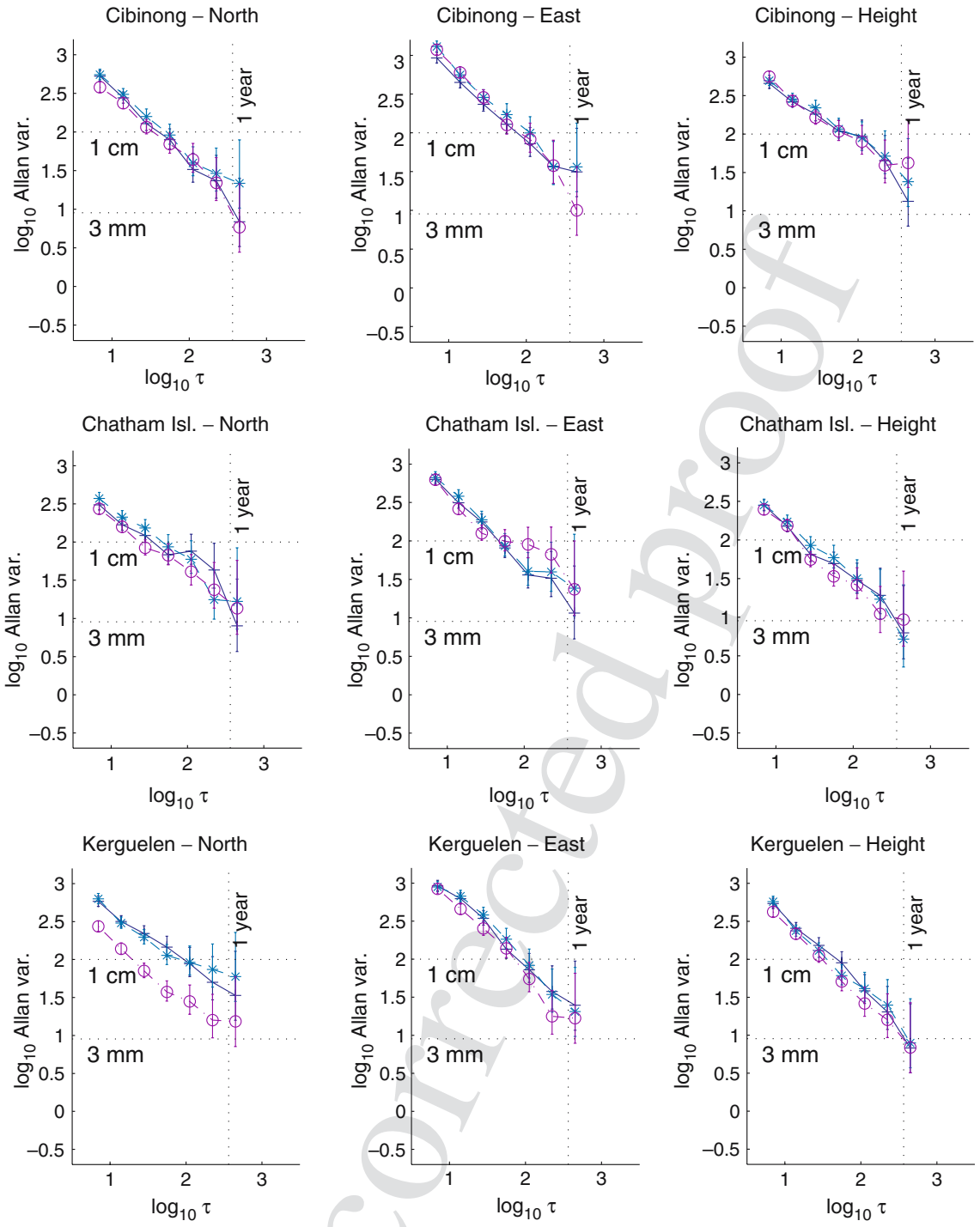

Fig. 2 Allan graphs in the local *N*,*E*,*U* frame of non-linear, non-seasonal DORIS station motion: CIBB, CHAB, and KERB. *Crosses* IGN-JPL, *stars* INASAN, *circles* LEGOS-CLS

The spectrum qualification obtained here for a few GPS stations analysed by a single AC are in agreement with results for the IGS network based on the combined time-series of stations derived by Feissel-Vernier and Le Bail (2006). The first principal component (PC1) explains over 80% of the non-linear signal for most of the stations. It has flicker noise for about two-third of the stations, and white noise for the remaining one-third of the stations. The second and third components (PC2 and PC3) explain less than 30% of the non-linear signal and

Journal: 190 MS: 88 CMS: GIVE CMS ☐ TYPESET ☐ DISK ☐ LE ☐ CP Disp.:2006/8/18 Pages: 25

Table 4 Spectral content and behaviour in the local N, E, U frame for three DORIS stations

Series	North			East			Height		
	Allan slope and noise type	Fisher test prob.	7-day Astd (mm)	Allan slope and noise type	Fisher test. prob.	7-day Astd (mm)	Allan slope and noise type	Fisher test prob.	7-day Astd (mm)
Cibinong (CIBB)									
IGN-JPL	-0.98 ± 0.03Wh	0.99	[21, 25]	-0.96 ± 0.02Wh	0.99	[28, 33]	-0.73 ± 0.03Wh	0.99	[20, 24]
INASAN	-0.90 ± 0.04Wh	0.99	[21, 26]	-1.03 ± 0.05Wh	0.99	[33, 39]	-0.72 ± 0.04Wh	0.99	[20, 24]
LEGOS-CLS	-0.72 ± 0.06Wh	0.94	[23, 27]	-0.67 ± 0.08Wh	0.98	[37, 43]	-0.82 ± 0.07Wh	0.99	[25, 29]
Chatham Island (CHAB)									
IGN-JPL	-0.75 ± 0.05Wh	0.99	[16, 19]	-0.96 ± 0.04Wh	0.99	[23, 28]	-0.94 ± 0.05Wh	0.99	[15, 19]
INASAN	-0.74 ± 0.04Wh	0.99	[17, 21]	-0.95 ± 0.05Wh	0.99	[24, 28]	-0.86 ± 0.05Wh	0.98	[16, 19]
LEGOS-CLS	-0.79 ± 0.02Wh	0.99	[14, 17]	-0.82 ± 0.11Wh	0.94	[22, 28]	-0.53 ± 0.04Fl	0.98	[14, 18]
Kerguelen (KERB)									
IGN-JPL	-0.71 ± 0.03Wh	0.99	[22, 27]	-0.94 ± 0.08Wh	0.99	[28, 33]	-0.99 ± 0.05Wh	0.99	[21, 25]
INASAN	-0.78 ± 0.07Wh	0.93	[23, 27]	-0.89 ± 0.10Wh	0.98	[27, 33]	-1.11 ± 0.05Wh	0.99	[22, 26]
LEGOS-CLS	-0.66 ± 0.06Wh	0.97	[13, 16]	-1.00 ± 0.06Wh	0.99	[24, 29]	-0.85 ± 0.07Wh	0.94	[15, 18]

The Allan slope is given with a 1σ uncertainty. Numbers in brackets give the 90% confidence interval of the "Allan standard deviation" for a 7-day sampling time. The fourth column is the probability of a satisfactory estimate of the Allan slope, given by the Fisher test
Wh white noise, *Fl* flicker noise type determination

Table 5 Spectral content and behaviour for three co-located DORIS and GPS stations decomposed into the time-like principal components PC1, PC2, and PC3

Series	PC1			PC2			PC3		
	Var (%)	Allan slope and noise type	7-day Astd (mm)	Var (%)	Allan slope and noise type	7-day Astd (mm)	Var (%)	Allan slope and noise type	7-day Astd (mm)
DORIS-CIBB									
IGN-JPL	47	-1.07 ± 0.05Wh	[29, 34]	28	-0.79 ± 0.04Wh	[21, 24]	25	-1.01 ± 0.03Wh	[21, 25]
INASAN	50	-1.09 ± 0.04Wh	[35, 41]	26	-0.76 ± 0.03Wh	[21, 25]	24	-0.90 ± 0.06Wh	[21, 25]
LEGOS-CLS	55	-1.01 ± 0.07Wh	[32, 38]	26	-0.88 ± 0.06Wh	[21, 25]	19	-0.89 ± 0.04Wh	[17, 21]
GPS-BAKO									
CODE	59	-0.15 ± 0.09Fl	[5, 7]	35	-0.16 ± 0.08Fl	[4, 5]	6	-0.31 ± 0.04Fl	[2, 3]
DORIS-CHAB									
IGN-JPL	52	-0.99 ± 0.08Wh	[22, 27]	28	-0.79 ± 0.05Wh	[17, 21]	20	-1.00 ± 0.05Wh	[15, 18]
INASAN	51	-0.95 ± 0.05Wh	[24, 30]	30	-0.82 ± 0.02Wh	[18, 22]	19	-1.11 ± 0.04Wh	[16, 19]
LEGOS-CLS	48	-0.82 ± 0.06Wh	[20, 24]	29	-0.67 ± 0.02Wh	[14, 18]	23	-0.92 ± 0.05Wh	[14, 17]
GPS-CHAT									
CODE	63	-0.09 ± 0.07Fl	[7, 8]	25	0.01 ± 0.04Fl	[4, 5]	12	-0.31 ± 0.08Fl	[3, 5]
DORIS-KERB									
IGN-JPL	47	-0.91 ± 0.10Wh	[27, 33]	30	-0.76 ± 0.03Wh	[22, 27]	23	-1.00 ± 0.05Wh	[22, 26]
INASAN	48	-0.95 ± 0.09Wh	[28, 34]	30	-0.81 ± 0.07Wh	[23, 27]	22	-1.07 ± 0.07Wh	[22, 27]
LEGOS-CLS	55	-0.98 ± 0.08Wh	[26, 31]	27	-1.00 ± 0.05Wh	[19, 23]	18	-0.81 ± 0.05Wh	[15, 18]
GPS-KERG									
CODE	50	-0.25 ± 0.04Fl	[8, 9]	36	-0.16 ± 0.09Fl	[5, 7]	14	-0.22 ± 0.04Fl	[4, 5]

Var (%) is the percentage of explained variance, the Allan slope is given with a 1σ uncertainty. Numbers in brackets give the 90% confidence interval of the "Allan standard deviation" for a 7-day sampling time
Wh white noise, *Fl* flicker noise type determination

have white noise for about half of the stations and flicker noise elsewhere.

4.3 Separating independent noise signatures by PCAT

One strength of the method proposed here is its ability to separate independent noises, which might be helpful in looking for hidden error sources. Figure 4 shows the PCAT decomposition for the DORIS HBKB station at Hartebeesthoek (Africa), from IGN-JPL, observed over 2000.6–2004.8. This shows the change in short-term scatter at the time when two more satellites were added in the DORIS constellation (2002.4). The time-series of N, E, U residuals are plotted in the upper part of Fig. 4. The noise reduction is visible in all three directions.

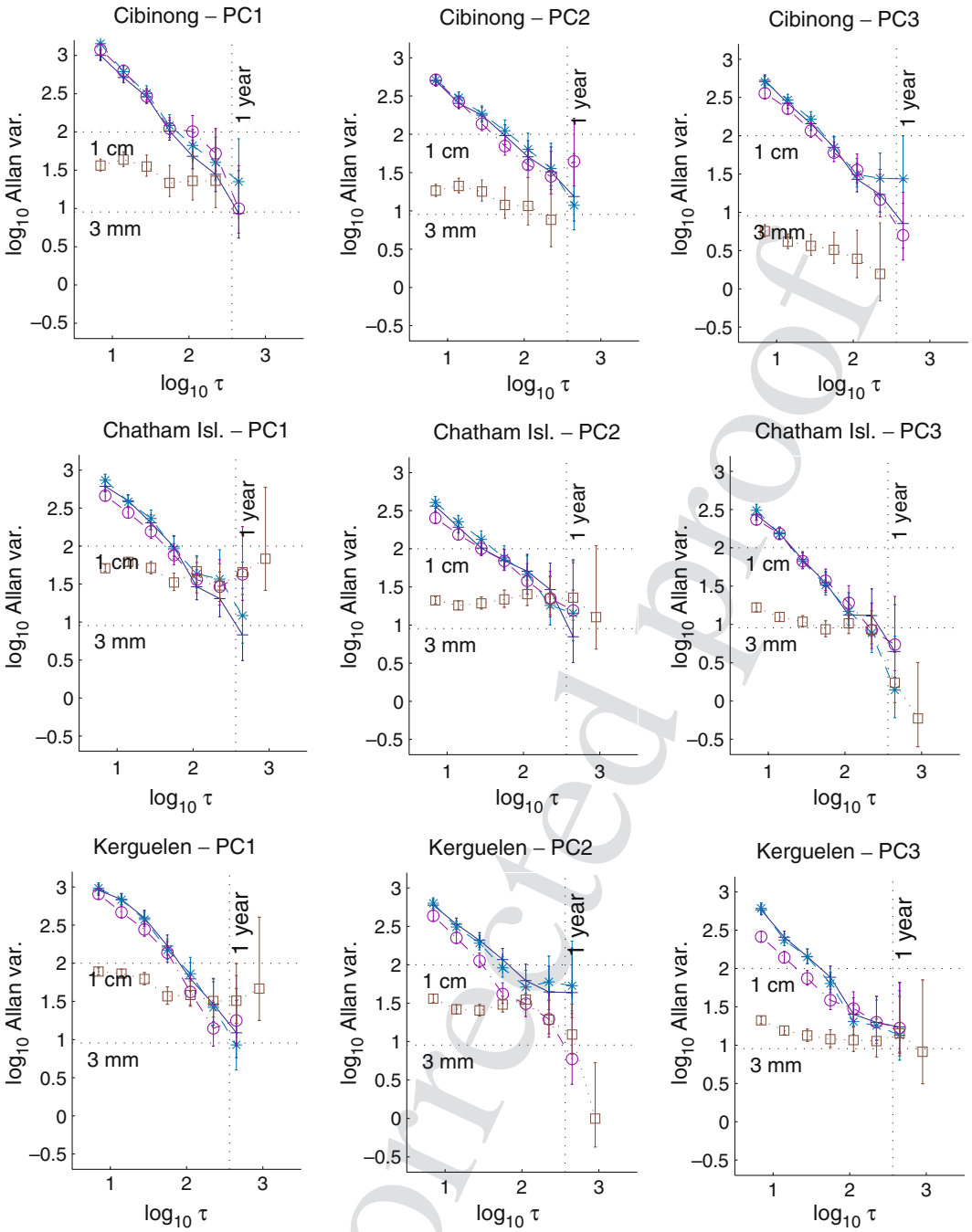

Fig. 3 Allan graphs of the principal component analysis in the time domain of non-linear, non-seasonal motions for co-located DORIS and GPS stations: CIBB/BAKO, CHAB/CHAT, and KERB/KERG. *Crosses* IGN-JPL, *stars* INASAN, *circles* LEGOS-CLS, *squares* CODE

When looking at the equivalent series in the time-eigenspace PC1, PC2, PC3, the first component PC1, which explains 49% of the signal, keeps the same short-term scatter, while the PC2 and PC3 components show the expected improvement. The projection factors of PC1, PC2, PC3 on the *N*, *E*, *U* directions are [0.21;0.97;−0.15], [0.98;-0.21;−0.03] and [0.07;0.14;0.99], respectively. Although the projection of PC1 is close to the East component, PCAT has succeeded in extracting a specific behaviour that was less apparent in the *N*, *E*, *U* frame. The peculiar PC1 behaviour is present for the three ACs, but it does not appear in the co-located GPS station HRAO, indicating that the noise in the East direction is dominated by an additional phenomenon that is still unmodelled in the DORIS analyses.

Journal: 190 MS: 88 CMS: GIVE CMS ☐ TYPESET ☐ DISK ☐ LE ☐ CP Disp.:2006/8/18 Pages: 25

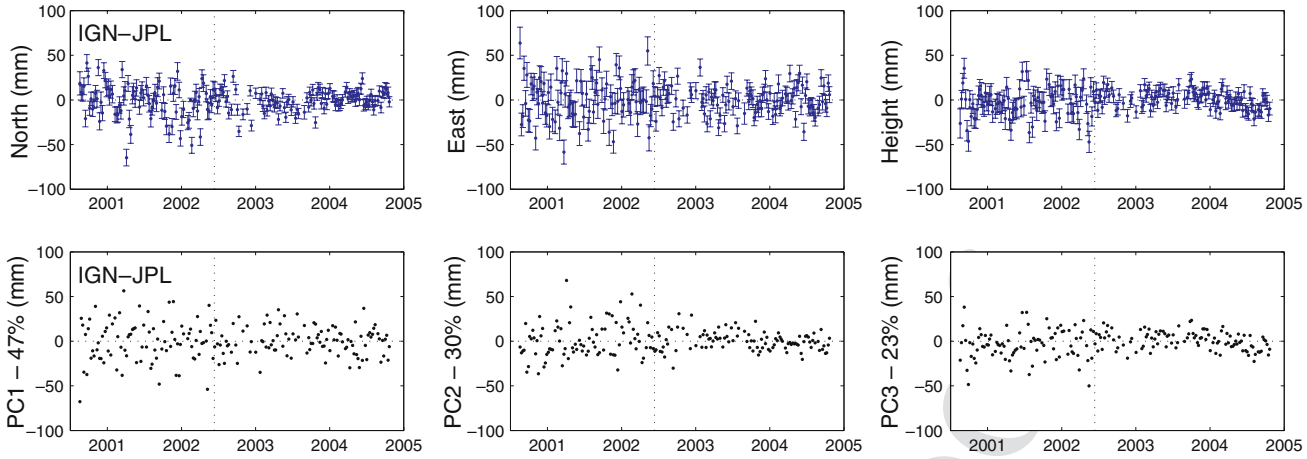

Fig. 4 PCAT of HBKB (Hartebeesthoek, Africa) station motion for IGN-JPL. *Top* PC_i time-series, *bottom* PC_i Allan graphs

5 DORIS network: spectral behaviour of position time-series

We now apply the time-series analysis to the IGN-JPL, INASAN, and LEGOS-CLS individual AC solutions for the whole DORIS network to derive the noise level and spectrum in the local frame (Sect. 5.1), and in the time-eigenspace obtained by PCAT (Sect. 5.2). Then we study how the N, E, U directions are affected by the independent noises derived in the time-eigenspace domain (Sect. 5.3).

5.1 Spectral behaviour in the local frame N, E, U

Prior to the analysis of the complete set of time-series of residuals, the level of cross-correlations between the N, E, U station time-series was checked. As expected, considering the even distribution of the network and of the satellite passes over the stations, the correlations are weak. They stay in the intervals $[-0.20; 0.25]$ for $[-0.35; 0.30]$, $[-0.30; 0.30]$ for IGN-JPL, INASAN, and LEGOS-CLS, respectively. The East–Up correlations are the smallest with a maximum of 0.2 in absolute value, while the North–East correlations are the largest, up to 0.35.

The values of the 7-day "Allan standard deviation" and type of noise of the well-observed stations' (C1) network are illustrated in Fig. 5 for the three ACs. The type of noise is derived from the Allan graph slope. It is symbolized by open circles for white noise, stars for flicker noise, and triangles in inconclusive cases.

The East component has the largest "Allan standard deviations": up to 50 mm for INASAN, 43 mm for IGN-JPL, and 41 mm for LEGOS-CLS, but the type of noise is white for all stations. The North and South components show 10–30 mm white noise, with a few exceptions. The North component shows an inconclusive spectrum in a few cases: OTTA (Ottawa, Canada) for the three ACs and SODA (Socorro, Mexico) for INASAN. In the height component, FAIA (Fairbanks, Alaska) shows an inconclusive spectrum for the three ACs, GREB (Greenbelt, USA) for IGN-JPL and INASAN, SPIB (Ny-Alesund, Norway) for INASAN, and AMTB (Amsterdam, France T.A.A.F.), CICB (Cibinong, Indonesia), PAQB (Papeete, French Polynesia), and YELB (Yellowknife, Canada) for LEGOS-CLS.

5.2 Spectral behaviour in the time-eigenspace

Although the empirical cross-correlations are weak on average, the motion components in the North, East, and height directions are not independent in principle, unlike the principal components derived by PCAT. Table 6 gives the results obtained for the first PCAT (PC1) for the whole network: percentage of explained Allan variance, type of noise (Fisher test is indicated by the probability for which the assumption of a linear drift is realistic), and "Allan standard deviation" for the 7-day sampling time.

The quality category of the time-series, defined in Sect. 2, is also listed in Table 6. It is pointed out that the series in the categories C2 or C3 are less suited for statistical analysis. Note that if the probability is lower than 0.8, that particular case must be reconsidered. The Allan graph can show the sum of noises or residual periodic signals. Results similar to those of Table 6, but for all three principal components, are plotted in Fig. 6 for the well-observed stations (C1 category). The graphs show 7-day "Allan standard deviation" in abscissae and the Allan graph slope in ordinates.

The dominant non-linear, non-seasonal signal of the PC1 series represents 40–60% of the total signal and

Journal: 190 MS: 88 CMS: GIVE CMS ☐ TYPESET ☐ DISK ☐ LE ☐ CP Disp.:2006/8/18 Pages: 25

Fig. 5 Spectral content and behaviour in the local frame of DORIS station non-linear motions for the three studied Analysis Centres. *Top* (*dark blue*) IGN-JPL, *middle* (*light blue*) INASAN, *bottom* (*pink*) LEGOS-CLS; *Circles* white noise, *stars* flicker noise, *triangles* inconclusive noise type determination

shows white noise. The stability for the 7-day sampling time is at the 10-45 mm level. PC2 represents 20–40% of the total signal and shows 10–40 mm white noise. PC3 represents 17–30% of the total signal and shows 10–28 mm white noise. Although, as explained in Sect. 3, the analysis strategies of the ACs have some differences, the agreement of statistics among the various solutions is quite close. Even including the C3 stations, for which the statistics are not expected to be robust, percentages of the explained variance and noise levels

Journal: 190 MS: 88 CMS: GIVE CMS ☐ TYPESET ☐ DISK ☐ LE ☐ CP Disp.:2006/8/18 Pages: 25

agree for the three ACs, within 8% and 10 mm, respectively.

The determinations of the noise type are in close agreement, too. As in the case of the study in the *N*, *E*, *U* frame, there are a few cases where the Allan graph slopes have intermediate values between −1 and 0, preventing a straightforward interpretation in terms of the noise spectrum. Fisher test probabilities are generally larger than 0.80. Most flicker noise diagnoses get a poor Fisher test probability, indicating that a linear model is not appropriate for the corresponding Allan graphs. As an example, OTTA (C1 category) gets an inconclusive noise type determination diagnosis, with a Fisher test value of 0.34–0.76 only.

For the first principal component (PC1) in Fig. 6, one can distinguish two populations in the case of IGN-JPL: stations clearly with white noise at the 15–45 mm level, and few stations around the flicker virtual border with a lower noise level, around 20 mm. OTTA shows inconclusive noise type determination. It is located on a very high (23 storey) building, which cannot be considered a stable monumentation for a geodetic instrument. The stations SPIB (Ny-Alesund, Norway) and SYOB (Syowa, Antarctica), in increasing order of Allan graph slope, are close to the virtual flicker border. These stations are high-latitude stations. The effect of station latitude on the quality of the positions time-series is further studied in Sect. 6.5.

For INASAN, the PC1 component has a behaviour similar to IGN-JPL : OTTA is an inconclusive noise type determination station and, SPIB and SYOB are close to the virtual flicker border. For LEGOS-CLS, OTTA also shows inconclusive spectrum on PC1, but contrary to IGN-JPL and INASAN, PC2 and PC3 show stations with inconclusive noise type determination. Our analysis suggests that the presence of white noise in the PC1 results from the lack of observations, masking the flicker noise, which is at a lower level. This may explain the fact that flicker noise appears with the increase of observations.

5.3 Projection of the PCATs in the local frame

The noise spectra, identified by the combined use of PCAT and Allan variance analysis, have the advantage of being statistically independent by design, but their drawback is that the directions in which these spectra are known have no particular physical meaning. To recover such understanding, we plotted (Fig. 7) the distribution of each of the PCAT eigenvectors in the *N*, *E*, *U* frame, together with the percentage of explained Allan variance for each of the PCATs, for the well-observed stations (C1).

PC1 has an explained Allan variance around 40–60%, and it is oriented on the East direction for the three ACs. We easily notice a lack of symmetry in this histogram, that may be related to the orientation of the satellites' passes. PC2 has a mixed North and height projection for IGN-JPL and INASAN, while it is clearly in the height component for LEGOS-CLS. The third principal component is directed by the height component for IGN-JPL and INASAN while, for LEGOS-CLS, the North component is the most significant direction. Note that the height component is strongly correlated with the modelling and estimation of the tropospheric correction and the clocks. The more subtle estimation made by IGN could be part of the explanation of these differences (Willis et al. 2003; Snajdrova et al. 2006).

6 Influence of geophysical, technical and observational factors on the station stability

In this section, we study the sensitivity of our stability diagnoses with some environmental factors: atmospheric loading (Sect. 6.1), antenna type (Sect. 6.2), number of DORIS satellites in the constellation (Sect. 6.3), technical quality of the station (Sect. 6.4), and latitude of the station (Sect. 6.5). We used the well-observed stations (C1) only.

6.1 Atmospheric loading

According to Williams et al. (2005), atmospheric loading has a first-order Gauss–Markov-like power spectrum that is white-like at low frequencies. The amplitude of atmospheric loading increases with latitude such that it is likely to be a major contributor to the GPS signals in the 10- to 100-day time-frame at high latitudes.

In a preliminary study, Le Bail et al. (2006) evaluated the contribution of atmospheric loading to station noise, based on the DORIS and GPS time-series at Krasnoyarsk (Russia) and Hartebeesthoek (Africa). They showed that the short-term atmospheric contribution has a level of 3 mm, which is similar to the precision level of GPS coordinates, while the DORIS coordinates precision is larger (15 mm). This implies that the effect can be seen in GPS results and not in DORIS ones.

Concerning the long-term atmospheric contribution, it has a white noise spectrum, at a much lower level than geodetic measurements: for the two stations, the "Allan standard deviations" at 1 year of the DORIS and GPS coordinates are at the level of 2–4 mm, while the amplitude of the atmospheric loading is at the level of 0.2–0.4 mm. Le Bail et al. (2006) conclude, then, that it is unlikely that atmospheric loading influences the long-

Journal: 190 MS: 88 CMS: GIVE CMS ☐ TYPESET ☐ DISK ☐ LE ☐ CP Disp.:2006/8/18 Pages: 25

Table 6 Spectral content and behaviour for the whole DORIS network decomposed into the time-like principal components PC1, PC2, and PC3

DORIS	IGN-JPL PC1					INASAN PC1					LEGOS-CLS PC1				
stations	Crit.	%Var	Allan spect.	Fisher test prob.	7-day AStd (mm)	Crit.	%Var	Allan spect.	Fisher test prob.	7-day AStd (mm)	Crit.	%Var	Allan spect.	Fisher test prob.	7-day AStd (mm)
ADEA	**C1**	**46**	**Wh**	**0.98**	**18**	**C1**	**44**	**Wh**	**0.99**	**19**	**C1**	**48**	**Wh**	**0.65**	**15**
ADEB	C3	50	Wh	0.99	14	C3	61	Wh	0.89	19	C3	60	In	0.65	18
AMSA	C3	49	Wh	0.98	30	**C1**	**44**	**Wh**	**0.82**	**28**	**C1**	**46**	**Wh**	**0.86**	**27**
AMSB						C3	56	Wh	0.96	27	C3	62	Wh	0.98	26
AMTB	C2	46	Wh	0.98	21	C3	48	Wh	0.99	24	**C1**	**49**	**Wh**	**0.95**	**24**
AREA	C3	49	Wh	0.97	36	C3	50	Wh	0.98	38	C3	57	Wh	0.97	40
AREB	C3	47	Wh	0.86	25	C3	52	Wh	0.79	25	C3	60	Wh	0.84	31
ARMA	C3	49	Wh	1.00	35	C3	49	Wh	1.00	40	C3	60	Wh	1.00	41
ASDB	**C1**	**52**	**Wh**	**1.00**	**34**	**C1**	**51**	**Wh**	**0.98**	**36**	**C1**	**54**	**Wh**	**1.00**	**36**
BADA	C2	47	Wh	1.00	26	C2	49	Wh	1.00	27	C2	59	Wh	1.00	25
BADB	C3	66	Wh	0.99	14						C3	51	Wh	0.85	9
CACB	C3	54	Wh	0.99	44	C2	51	Wh	0.99	47	C2	50	Wh	0.94	38
CADB	C3	60	Wh	0.97	24						C3	59	Wh	0.85	27
CHAB	**C1**	**52**	**Wh**	**1.00**	**25**	**C1**	**51**	**Wh**	**1.00**	**27**	**C1**	**48**	**Wh**	**0.95**	**21**
CIBB	**C1**	**47**	**Wh**	**1.00**	**32**	**C1**	**50**	**Wh**	**1.00**	**38**	**C1**	**55**	**Wh**	**0.99**	**35**
CICB	**C1**	**41**	**Wh**	**0.99**	**19**	**C1**	**45**	**Wh**	**1.00**	**23**	**C1**	**51**	**Wh**	**0.99**	**22**
COLA	C3	48	Wh	1.00	24	C3	49	Wh	0.96	27	C3	57	Wh	0.98	27
CROB	C3	55	Wh	0.88	14						C3	53	Wh	0.88	14
DAKA	**C1**	**54**	**Wh**	**0.96**	**32**	**C1**	**56**	**Wh**	**0.96**	**34**	**C1**	**55**	**Wh**	**1.00**	**31**
DIOA	C2	50	Wh	1.00	31	C2	52	Wh	0.99	31	C2	56	Wh	1.00	31
DJIA	**C1**	**49**	**Wh**	**0.95**	**27**	**C1**	**50**	**Wh**	**0.99**	**28**	**C1**	**54**	**Wh**	**0.99**	**26**
DJIB	C3	46	Wh	1.00	31	**C1**	**48**	**Wh**	**0.99**	**38**	**C1**	**47**	**Wh**	**1.00**	**27**
EASA	**C1**	**47**	**Wh**	**1.00**	**35**	**C1**	**46**	**Wh**	**1.00**	**36**	**C1**	**54**	**Wh**	**0.94**	**35**
EASB	**C1**	**38**	**Wh**	**0.91**	**19**	C3	45	Wh	0.80	22	**C1**	**58**	**Wh**	**0.97**	**24**
EVEB	C3	54	Wh	1.00	33	C3	55	Wh	1.00	35	C3	66	Wh	1.00	36
FAIA	**C1**	**39**	**Wh**	**1.00**	**19**	**C1**	**40**	**Wh**	**1.00**	**19**	**C1**	**47**	**Wh**	**0.98**	**19**
FAIB	C3	41	Wh	1.00	17	C3	43	Wh	1.00	17	C3	47	In	0.32	13
FUTB	C3	41	Wh	0.99	21	**C1**	**45**	**Wh**	**0.92**	**23**	C2	56	Wh	1.00	25
GALA	C3	56	Wh	0.99	28	C3	55	Wh	0.98	33	C3	56	Wh	0.95	34
GAVB	C3	49	Wh	0.81	13	C3	45	Wh	0.64	11	C3	44	Wh	0.74	12
GOLA	C3	53	Wh	0.93	42	C3	56	Wh	0.67	54	C3	66	Wh	0.72	48
GOMA	C3	56	Wh	0.98	30	C3	54	Wh	0.96	30	C3	47	Wh	0.83	23
GOMB	C2	51	Wh	1.00	22	**C1**	**50**	**Wh**	**1.00**	**23**	C2	55	Wh	0.97	23
GREB	**C1**	**42**	**Wh**	**0.99**	**17**	**C1**	**42**	**Wh**	**1.00**	**17**	**C1**	**54**	**Wh**	**0.83**	**18**
GUAB	**C1**	**53**	**Wh**	**0.97**	**31**	**C1**	**51**	**Wh**	**1.00**	**32**	**C1**	**59**	**Wh**	**0.99**	**32**
HBKA	**C1**	**50**	**Wh**	**0.99**	**26**	**C1**	**52**	**Wh**	**0.94**	**26**	**C1**	**53**	**Wh**	**1.00**	**24**
HBKB	**C1**	**47**	**Wh**	**1.00**	**21**	**C1**	**46**	**Wh**	**0.99**	**24**	**C1**	**63**	**Wh**	**0.89**	**23**
HBLA	**C1**	**45**	**Wh**	**0.89**	**27**	**C1**	**42**	**Wh**	**0.81**	**26**	**C1**	**53**	**Wh**	**0.95**	**23**
HELA	**C1**	**56**	**Wh**	**0.95**	**35**	**C1**	**61**	**Wh**	**0.93**	**38**	**C1**	**50**	**Wh**	**0.99**	**30**
HELB	**C1**	**55**	**Wh**	**0.94**	**32**	**C1**	**54**	**Wh**	**0.96**	**31**	**C1**	**55**	**Wh**	**0.95**	**31**
HEMB	C3	56	Wh	1.00	16	C3	55	Wh	0.79	20	C3	68	Wh	0.96	20
HUAA	C3	62	Wh	0.67	31	C3	51	Wh	0.92	31	C3	57	Wh	0.91	28
IQUB	C3	54	Wh	0.84	42	C3	53	Wh	0.71	45					
JIUB	C3	49	Wh	0.88	38										
KERA	C3	62	Wh	0.74	41	C3	59	Wh	0.65	44	C3	60	Wh	0.70	31
KERB	**C1**	**47**	**Wh**	**0.98**	**30**	**C1**	**48**	**Wh**	**0.98**	**31**	**C1**	**54**	**Wh**	**0.99**	**28**
KESB	C2	49	Wh	0.98	23	C3	54	Wh	0.95	23	C2	55	Wh	0.88	21
KITA	C3	54	Wh	0.92	22	C3	55	Wh	0.99	26	C3	61	Wh	1.00	27
KITB	C3	50	Wh	0.95	26	C3	47	Wh	1.00	28	C2	66	Wh	0.98	31
KIUB	**C1**	**51**	**Wh**	**1.00**	**18**	**C1**	**55**	**Wh**	**0.99**	**21**	**C1**	**67**	**Wh**	**0.96**	**21**
KOKA	**C1**	**55**	**Wh**	**1.00**	**36**	**C1**	**55**	**Wh**	**1.00**	**40**	**C1**	**52**	**Wh**	**1.00**	**31**
KOLB	C3	46	Wh	0.84	16	C3	50	Wh	0.90	16	C3	45	Wh	0.88	17
KRAB	C2	43	Wh	0.99	20	C2	42	Wh	0.99	19	**C1**	**39**	**Wh**	**1.00**	**15**
KRUB	C3	45	Wh	1.00	32	C2	46	Wh	1.00	32	**C1**	**52**	**Wh**	**0.96**	**31**
LIBA	**C1**	**57**	**Wh**	**1.00**	**31**	**C1**	**57**	**Wh**	**0.97**	**34**	**C1**	**60**	**Wh**	**1.00**	**34**
LIBB	**C1**	**54**	**Wh**	**1.00**	**26**	**C1**	**53**	**Wh**	**0.99**	**29**	**C1**	**62**	**Wh**	**0.98**	**26**
LIFB	C3	59	Wh	0.86	40	C3	54	Wh	0.98	51					
MAHB	**C1**	**41**	**Wh**	**1.00**	**26**	C3	42	Wh	0.96	32	**C1**	**57**	**Wh**	**0.96**	**27**

Journal: **190** MS: **88** CMS: **GIVE CMS** ☐ TYPESET ☐ DISK ☐ LE ☐ CP Disp.:**2006/8/18** Pages: **25**

Table 6 continued

MANA	C3	51	Wh	1.00	38	**C1**	**52**	**Wh**	**1.00**	**40**	**C1**	**56**	**Wh**	**0.91**	**36**
MANB	C3	43	Wh	0.77	21	C3	50	In	0.92	22	C3	48	Wh	0.95	30
MARA	**C1**	**56**	**Wh**	**0.99**	**39**	**C1**	**54**	**Wh**	**1.00**	**42**	**C1**	**56**	**Wh**	**0.99**	**34**
MARB	C3	45	Wh	0.99	22	C3	46	Wh	0.94	23	C3	53	Wh	1.00	21
MATB	C3	51	Wh	0.82	18						C3	60	Wh	0.42	13
META	**C1**	**52**	**Wh**	**1.00**	**31**	**C1**	**52**	**Wh**	**1.00**	**33**	**C1**	**51**	**Wh**	**1.00**	**26**
METB	C2	40	Wh	0.67	16	C3	45	Wh	0.95	19	**C1**	**54**	**Wh**	**0.99**	**21**
MORA	C3	45	Wh	1.00	31	C3	51	Wh	1.00	37	C3	54	Wh	1.00	35
MORB	C3	50	Wh	0.99	22	C3	49	Wh	0.95	26	C3	55	Wh	0.99	29
MSOB	**C1**	**43**	**Wh**	**0.97**	**28**	**C1**	**45**	**Wh**	**0.96**	**28**	**C1**	**50**	**Wh**	**0.98**	**27**
MSPB	C3	44	Wh	0.97	14						C3	54	Wh	0.83	17
NOUA	**C1**	**47**	**Wh**	**1.00**	**34**	**C1**	**48**	**Wh**	**1.00**	**35**	**C1**	**54**	**Wh**	**1.00**	**36**
NOUB	C3	59	Wh	0.78	40	C3	67	Wh	0.69	44	C3	67	Wh	0.60	32
ORRA	C3	60	Wh	1.00	52	C3	51	Wh	1.00	47	C3	60	Wh	0.97	48
ORRB	C3	53	Wh	0.95	48	C3	50	Wh	0.91	47	C3	51	Wh	0.88	44
OTTA	**C1**	**46**	**In**	**0.68**	**22**	**C1**	**45**	**In**	**0.76**	**24**	**C1**	**49**	**In**	**0.34**	**23**
OTTB	C3	46	Wh	1.00	26	C3	45	Wh	1.00	26	C3	51	Wh	1.00	24
PAPB	C3	47	Wh	0.98	31	C3	48	Wh	0.98	37	C3	44	Wh	0.94	39
PAQB	**C1**	**44**	**Wh**	**0.93**	**25**	**C1**	**47**	**Wh**	**0.65**	**29**	**C1**	**53**	**Wh**	**1.00**	**29**
PASB	C3	56	Wh	0.65	31	C3	57	Wh	0.48	32	C3	54	Wh	0.95	21
PDLB	C3	51	Wh	0.94	39	C3	53	Wh	0.84	39	C3	59	Wh	0.85	36
PDMB	**C1**	**45**	**Wh**	**0.97**	**19**	C3	53	Wh	0.91	22	**C1**	**60**	**Wh**	**0.98**	**22**
PURA	C2	47	Wh	1.00	32	C2	50	Wh	1.00	35	C2	51	Wh	1.00	30
RAQB	C2	45	Wh	1.00	28	C2	46	Wh	1.00	28	C2	47	Wh	0.97	30
REUA	**C1**	**57**	**Wh**	**1.00**	**32**	**C1**	**57**	**Wh**	**1.00**	**37**	**C1**	**60**	**Wh**	**0.86**	**31**
REUB	**C1**	**52**	**Wh**	**1.00**	**25**	**C1**	**51**	**Wh**	**1.00**	**27**	**C1**	**66**	**Wh**	**1.00**	**27**
REYA	**C1**	**46**	**Wh**	**0.96**	**22**	**C1**	**49**	**Wh**	**0.96**	**23**	**C1**	**40**	**Wh**	**0.99**	**19**
REYB	**C1**	**43**	**Wh**	**0.94**	**19**	**C1**	**43**	**Wh**	**0.95**	**18**	**C1**	**48**	**Wh**	**0.56**	**17**
REZB	C3	56	Wh	0.51	13										
RIDA	C3	47	Wh	1.00	28	C2	48	Wh	1.00	30	C2	51	Wh	0.86	27
RIOA	C3	40	Wh	0.85	22	C3	40	Wh	0.70	23	C3	47	Wh	0.90	15
RIOB	**C1**	**41**	**Wh**	**0.96**	**26**	**C1**	**42**	**Wh**	**0.98**	**27**	**C1**	**42**	**Wh**	**0.98**	**21**
RIPB	**C1**	**49**	**Wh**	**0.99**	**21**	**C1**	**52**	**Wh**	**0.90**	**24**	**C1**	**52**	**Wh**	**1.00**	**19**
ROTA	C2	39	Wh	0.96	17	**C1**	**38**	**Wh**	**1.00**	**16**	**C1**	**46**	**Wh**	**1.00**	**17**
SAKA	C3	44	Wh	1.00	27	C3	46	Wh	0.99	29	C3	44	Wh	1.00	22
SAKB	C3	51	Wh	0.89	14						C3	54	Wh	0.83	13
SALB	C3	64	Wh	1.00	20	C3	55	Wh	0.98	19	C3	68	Wh	0.99	19
SAMB	C3	46	Wh	0.99	48	**C1**	**47**	**Wh**	**1.00**	**53**	**C1**	**48**	**Wh**	**1.00**	**43**
SANA	C3	42	Wh	0.97	35	C3	45	Wh	0.99	38	C3	43	Wh	1.00	37
SANB	**C1**	**54**	**Wh**	**0.85**	**19**	C3	61	Wh	0.72	24	**C1**	**58**	**Wh**	**0.79**	**20**
SAOB	C3	49	Wh	1.00	37	C3	47	Wh	1.00	41	C3	46	Wh	1.00	41
SODA	C3	59	Wh	0.90	35	**C1**	**44**	**In**	**0.43**	**25**	**C1**	**45**	**Wh**	**0.39**	**30**
SODB	C3	40	Wh	0.99	22	C3	44	Wh	1.00	26	C2	64	Wh	1.00	30
SPIA	**C1**	**38**	**Wh**	**0.98**	**18**	**C1**	**40**	**Wh**	**1.00**	**19**	**C1**	**42**	**Wh**	**0.82**	**14**
SPIB	**C1**	**40**	**Wh**	**0.96**	**14**	**C1**	**40**	**Wh**	**0.88**	**15**	**C1**	**55**	**Wh**	**0.99**	**20**
SPJB	C3	55	Wh	0.94	13	C3	62	Wh	0.83	12	C3	72	In	0.88	27
STJB	**C1**	**43**	**Wh**	**1.00**	**18**	**C1**	**46**	**Wh**	**0.96**	**16**	**C1**	**49**	**Wh**	**0.99**	**20**
SYOB	**C1**	**45**	**Wh**	**1.00**	**16**	**C1**	**43**	**Wh**	**0.99**	**16**	**C1**	**48**	**Wh**	**1.00**	**16**
SYPB	**C1**	**39**	**Wh**	**0.80**	**14**	**C1**	**38**	**Wh**	**0.86**	**15**	**C1**	**48**	**Wh**	**0.92**	**14**
TANB	C3	48	Wh	0.65	38	C3	44	Wh	0.57	37					
THUB	C3	58	Wh	0.84	9	C3	52	Wh	0.99	9	C3	47	Wh	0.99	9
TLHA	**C1**	**50**	**Wh**	**1.00**	**24**	**C1**	**52**	**Wh**	**1.00**	**27**	**C1**	**53**	**Wh**	**0.99**	**24**
TLSA	**C1**	**52**	**Wh**	**0.99**	**28**	**C1**	**53**	**Wh**	**1.00**	**29**	**C1**	**55**	**Wh**	**1.00**	**28**
TRIA	**C1**	**50**	**Wh**	**1.00**	**29**	**C1**	**50**	**Wh**	**1.00**	**31**	**C1**	**52**	**Wh**	**1.00**	**28**
TRIB	**C1**	**41**	**Wh**	**0.93**	**15**	C3	42	Wh	1.00	18	C3	50	Wh	0.85	18
WALA	**C1**	**50**	**Wh**	**1.00**	**41**	C2	48	Wh	0.98	42	**C1**	**56**	**Wh**	**1.00**	**38**
YARA	**C1**	**49**	**Wh**	**0.99**	**32**	**C1**	**48**	**Wh**	**1.00**	**34**	**C1**	**52**	**Wh**	**0.98**	**29**
YARB	**C1**	**43**	**Wh**	**0.98**	**20**	**C1**	**45**	**Wh**	**0.95**	**19**	**C1**	**52**	**Wh**	**0.99**	**21**
YASB	C3	44	Wh	0.85	12						C3	63	Wh	0.82	14
YELA	**C1**	**47**	**Wh**	**1.00**	**21**	**C1**	**46**	**Wh**	**1.00**	**21**	**C1**	**44**	**Wh**	**0.99**	**19**
YELB	**C1**	**42**	**Wh**	**0.97**	**12**	C3	44	Wh	0.93	12	**C1**	**48**	**Wh**	**0.81**	**13**

%Var is the percentage of explained variance. Bold values are of best-observed stations (C1). The fourth column is the probability of a satisfactory estimate of the Allan slope, given by the Fisher test
Wh white noise, *Fl* flicker noise, *In* inconclusive noise type determination

Journal: 190 MS: 88 CMS: GIVE CMS ☐ TYPESET ☐ DISK ☐ LE ☐ CP Disp.:2006/8/18 Pages: 25

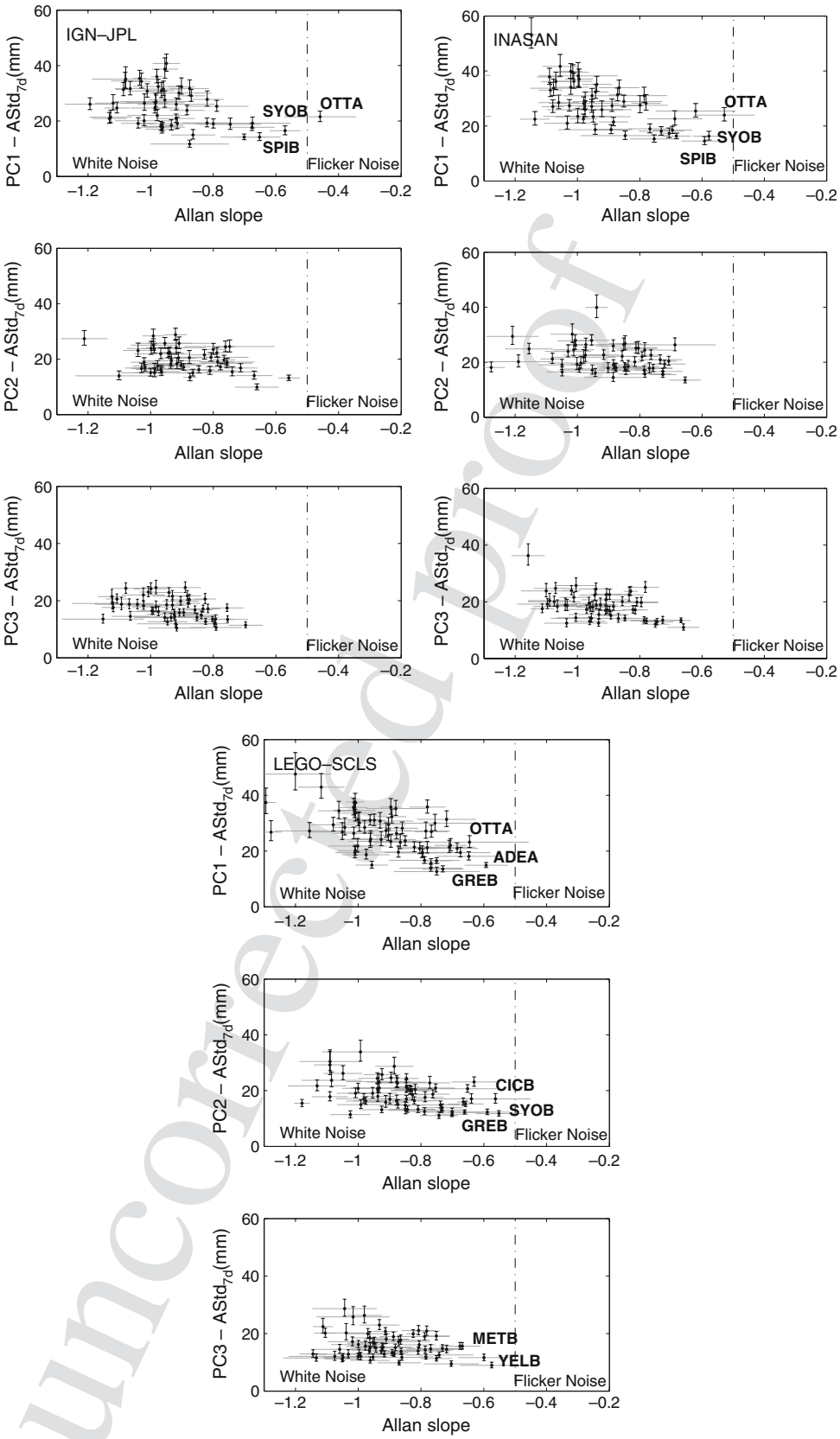

Fig. 6 Principal component analysis in the time domain of DORIS non-linear, non-seasonal motion of the well-observed stations (C1). *Top left* IGN-JPL, *top right* INASAN, *bottom* LEGOS-CLS. The names of stations with noise type closer to flicker noise are *printed*

Journal: **190** MS: **88** CMS: **GIVE CMS** ☐ TYPESET ☐ DISK ☐ LE ☐ CP Disp.:**2006/8/18** Pages: **25**

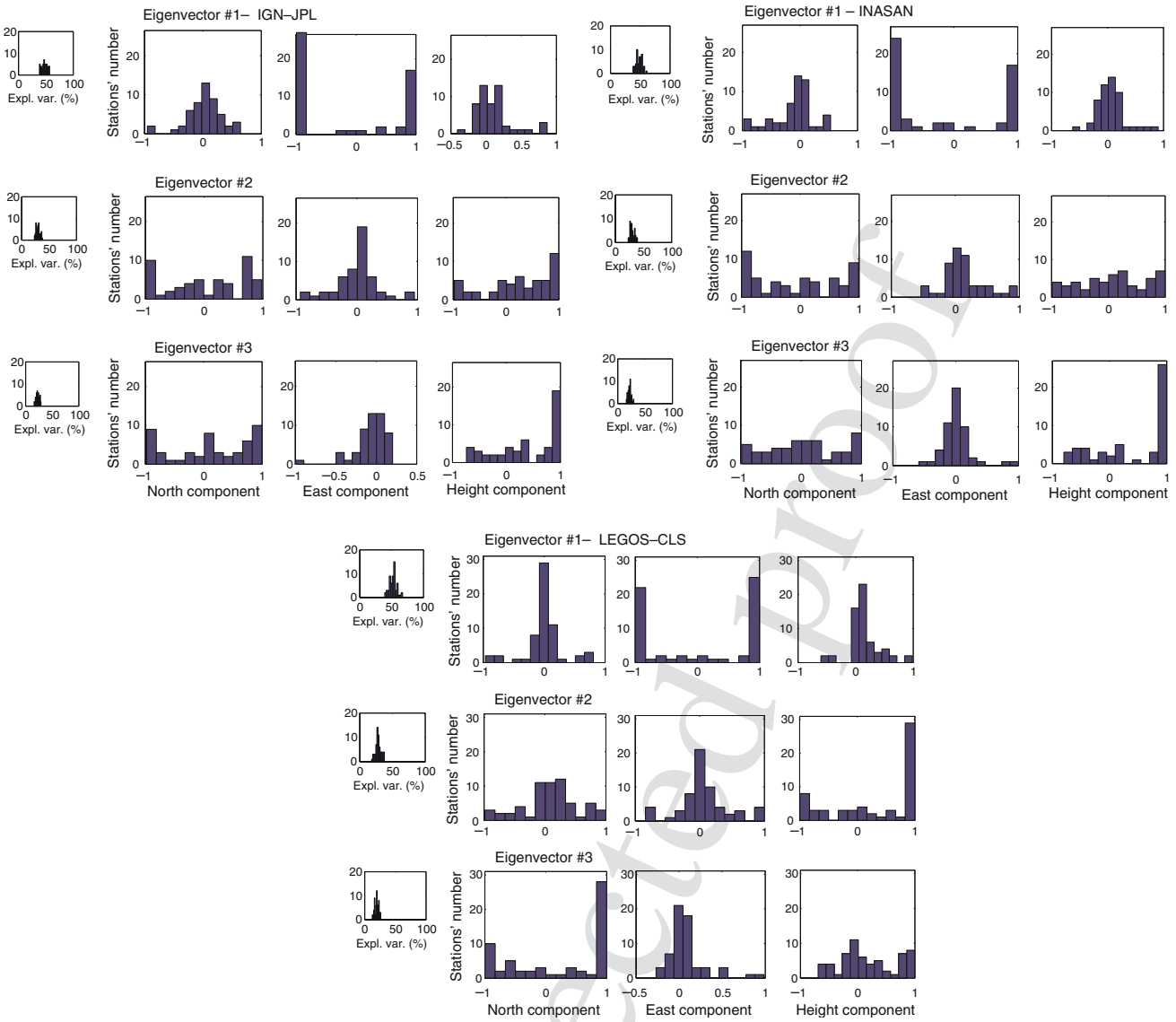

Fig. 7 Histograms of percentage of explained variance of each PC and projection of the PCAT eigenvectors in the local *N*,*E*,*U* frame, for the set of best observed stations (C1). *Top left* IGN-JPL, *top right* INASAN, *bottom* LEGOS-CLS

term stability of the terrestrial reference frame derived from series of station coordinates.

6.2 Antenna type

When studying the stability of the DORIS observing system, one has to consider the global network evolution, both in the ground and space segments. The DORIS ground-beacons may be equipped with one of two types of antennas, Alcatel (station names ending with A) or Starec (station names ending with B). The Starec antennas offer several improvements with respect to the original Alcatel model, in particular, a better-defined phase centre location (to within 1 vs. 5 mm for the Alcatel antennas) and a slimmer and more rigid design allowing a more precise survey and centring (Fagard 2006). As such, the Starec antennas are expected to have a better stability than the Alcatel ones (Fagard 2006). This type of antenna was installed in the course of the recent station rejuvenation project.

At the same time, the number of observation satellites in the DORIS constellation changed. In the course of the year 2002, the number of satellites taken into account in station positioning analysis, increased from three (SPOT-2, SPOT-4, and TOPEX/Poseidon) to five (ENVISAT and SPOT-5 missions were successful) until November 2004, when the DORIS data on-board

Journal: 190 MS: 88 CMS: GIVE CMS ☐ TYPESET ☐ DISK ☐ LE ☐ CP Disp.:2006/8/18 Pages: 25

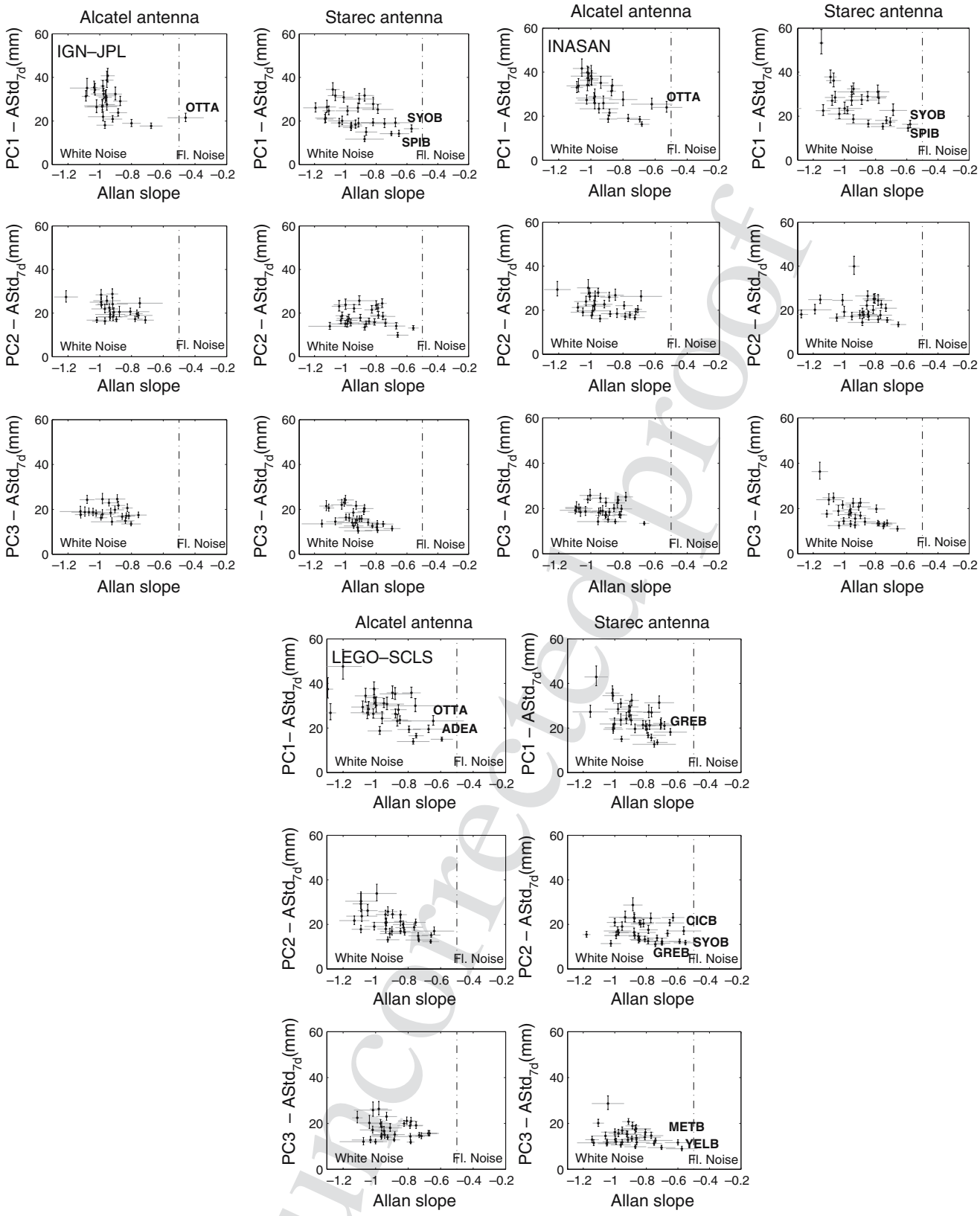

Fig. 8 Type and level of noise in DORIS station non-linear, non-seasonal motion. *Top left* IGN-JPL, *top right* INASAN, *bottom* LEGOS-CLS. *Left graphs* stations equipped with an Alcatel antenna (45 for the three ACs); *right graphs* stations equipped with a Starec antenna (73 for IGN-JPL, 65 for INASAN, 69 for LEGOS-CLS)

Journal: **190** MS: **88** CMS: **GIVE CMS** ☐ TYPESET ☐ DISK ☐ LE ☐ CP Disp.:**2006/8/18** Pages: **25**

TOPEX/Poseidon ended. Note that with the new generation of satellite receivers (Jason-1, ENVISAT, and SPOT-5), it is possible to get more data per station using the dual-channel capability. Despite the efforts made to correct a posteriori the Jason-1 oscillator instabilities in the analyses (Willis et al. 2004; Lemoine and Capdeville 2006), these observations cannot be used for geodetic positioning.

Figure 8 shows the stability results of Fig. 6, separately for Alcatel and Starec antenna types. The plotted quantities are 7-day "Allan standard deviations" in abscissae and Allan graph slopes in ordinates. The noise is slightly larger for the Alcatel antennas than for the Starec ones, which confirms the network administrators' expectations. The respective noise levels of the principal component in time ($PC1$) are 20–45 and 10–35 mm. Results for IGN-JPL and INASAN are more compatible with a white noise spectrum for the Alcatel antenna. For LEGOS-CLS, the noise spectrum is unaffected.

6.3 Number of DORIS satellites

The numbers of available DORIS satellites were three over 1998.0–2002.4 and five over 2002.4–2004.8. To study the impact of this increase in the amount of data collected, we selected eight well-observed stations with long time-series before and after 2002.4. The selected stations and the start of their observing periods are:

- ASDB (Ascension, U.K. South Atlantic Ocean): 1999.4
- CHAB (Chatham Island, New Zealand): 1999.3
- LIBB (Libreville, Gabon): 1999.2
- PAQB (Papeete, French Polynesia): 1998.6
- REUB (La Réunion, France): 1999.0
- REYB (Reykjavik, Iceland): 1998.7
- SYPB (Syowa, Antarctica): 1999.1
- TLHA (Toulouse, France): 1998.0. TLHA is the only station with an Alcatel antenna in this list.

Results are shown in Table 7. A decrease by about a factor of 2 is found at all stations for the five-satellite data, in agreement with the evaluations of Tavernier et al. (2006). The white noise spectrum in all three principal components in time is confirmed.

6.4 Technical quality of the station

To assess more precisely the quality of the antenna support at all DORIS sites, Fagard (2006) define a criteria for site quality (quality of equipment, reference point stability, reliability of power supply, and quality of station-coordinates time series) in order to identify a set of reference stations with accurate coordinates contributing to ITRF. The DORIS network ground-beacons are installed and renovated by the *Service d'Installation et de Maintenance des Balises* DORIS installation and maintenance department (IGN/SIMB) group, which can quantify all the characteristics of each monument.

An antenna stability criterion is built on the basis of all elements in the antenna support that may contribute to the antenna instability: the more elements there are between the antenna and the ground, the higher the risk of experiencing an antenna reference point (ARP) and/or phase centre displacement in the long term. This criterion is called instability degree (ID). The higher the ID, the less stable the antenna is expected to be. This ID is determined by Fagard (2006) on the basis of the technical quality of the antenna, supporting plate, plate assembly, nature of the primary and secondary supports (concrete pillar, metal tower, connected to the ground or to a building, etc.). This index represents the technical quality of the ground segment. It takes into account the monument quality without any consideration of temporal evolution or observation span.

To compare the ID of the DORIS stations with our results, we define a *stability index* (SI) as follows.

$$\begin{aligned} \mathrm{SI} = \frac{1}{3}\big(&\mathrm{Var}_1 \times (\mathrm{Aslope}_1 + \mathrm{Astd}_1) + \mathrm{Var}_2 \\ &\times (\mathrm{Aslope}_2 + \mathrm{Astd}_2) + \mathrm{Var}_3 \\ &\times (\mathrm{Aslope}_3 + \mathrm{Astd}_3)\big) \end{aligned} \tag{9}$$

where Var_i is the percentage of explained Allan variance of the ith PCAT component, Aslope_i is the Allan slope estimate of the ith PCAT component and Astd_i is the "Allan standard deviation" at 7 days of the ith PCAT component. With this definition, the less stable a station time-series of positions is, the higher will be the SI.

The technical ID are compared with our SI in Fig. 9, only considering the stations in the C1 category. The stations with Alcatel and Starec antennas are identified by different symbols (circles and triangles, respectively). The Alcatel antenna values are larger than the Starec antenna ones for both indices, and also more scattered. Thus, the lines mark the regression band between the two parameters corresponding to the two-sigma region of confidence surrounding the fit for the Starec antenna values only.

The stations with Starec antenna that are not in the band regression with a low statistical stability in spite of a small antenna ID, are Ascension (ASDB, U.K. South Atlantic Ocean) and Syowa (SYOB, Antarctica) for the three ACs, Ny-Alesund (SPIB, Norway) for IGN-JPL and INASAN, Santa Maria (SAMB, Portugal Azores) for INASAN and LEGOS-CLS, Mount Stromlo

Journal: 190 MS: 88 CMS: GIVE CMS ☐ TYPESET ☐ DISK ☐ LE ☐ CP Disp.:2006/8/18 Pages: 25

Table 7 Spectral content and behaviour for eight DORIS stations decomposed into the time-like principal components PC1, PC2, and PC3

Series	PC1			PC2			PC3		
	Var (%)	Allan slope and noise type	7-day Astd (mm)	Var (%)	Allan slope and noise type	7-day Astd (mm)	Var (%)	Allan slope and noise type	7-day Astd (mm)
ASDB									
IGN-JPL (1)	54	−1,25 ± 0.03**Wh**	40	25	−0.97 ± 0.12**Wh**	25	21	−1.08 ± 0.14**Wh**	25
IGN-JPL (2)	49	−0.98 ± 0.07**Wh**	**25**	33	−0.85 ± 0.09**Wh**	**21**	18	−1.21 ± 0.09**Wh**	**16**
INASAN (1)	52	−1.16 ± 0.02**Wh**	41	26	−0.80 ± 0.05**Wh**	27	21	−1.04 ± 0.10**Wh**	26
INASAN (2)	47	−0.86 ± 0.09 Wh	**25**	32	−1.06 ± 0.19**Wh**	**22**	21	−1.22 ± 0.06**Wh**	**20**
LEGOS-CLS (1)	62	−1.10 ± 0.06**Wh**	40	24	−0.92 ± 0.12**Wh**	23	14	−1.15 ± 0.04**Wh**	19
LEGOS-CLS (2)	53	−0.92 ± 0.07**Wh**	**30**	34	−0.67 ± 0.06**Wh**	**22**	13	−0.94 ± 0.11**Wh**	**15**
CHAB									
IGN-JPL (1)	49	−0.86 ± 0.05**Wh**	29	29	−0.91 ± 0.07**Wh**	25	22	−1.07 ± 0.05**Wh**	21
IGN-JPL (2)	64	−0.87 ± 0.07**Wh**	**19**	19	−0.82 ± 0.09**Wh**	**11**	18	−1.04 ± 0.08**Wh**	**10**
INASAN (1)	49	−0.89 ± 0.08**Wh**	32	31	−0.89 ± 0.09**Wh**	25	20	−1.13 ± 0.02**Wh**	22
INASAN (2)	60	−0.78 ± 0.17**Wh**	**16**	23	−0.91 ± 0.06**Wh**	**11**	17	−0.88 ± 0.06**Wh**	**10**
LEGOS-CLS (1)	47	−0.89 ± 0.02**Wh**	28	28	−0.94 ± 0.11**Wh**	20	25	−1.02 ± 0.10**Wh**	20
LEGOS-CLS (2)	45	−1.07 ± 0.10**Wh**	**15**	34	−0.81 ± 0.10**Wh**	**13**	21	−1.15 ± 0.05**Wh**	**11**
LIBB									
IGN-JPL (1)	56	−1.19 ± 0.13**Wh**	31	26	−1.10 ± 0.11**Wh**	23	17	−1.05 ± 0.07**Wh**	18
IGN-JPL (2)	49	−0.94 ± 0.10**Wh**	**17**	32	−1.00 ± 0.06**Wh**	**13**	19	−1.06 ± 0.10**Wh**	**11**
INASAN (1)	56	−1.25 ± 0.12**Wh**	34	26	−0.97 ± 0.10**Wh**	22	18	−1.02 ± 0.05**Wh**	20
INASAN (2)	45	−1.21 ± 0.06**Wh**	**17**	31	−0.99 ± 0.13**Wh**	**12**	24	−1.09 ± 0.08**Wh**	**12**
LEGOS-CLS (1)	62	−0.99 ± 0.03**Wh**	30	22	−1.09 ± 0.21**Wh**	17	16	−0.90 ± 0.06**Wh**	15
LEGOS-CLS (2)	63	−0.95 ± 0.07**Wh**	**18**	23	−1.15 ± 0.05**Wh**	**12**	14	−1.10 ± 0.11**Wh**	**9**
PAQB									
IGN-JPL (1)	43	−0.96 ± 0.09**Wh**	30	30	−1.08 ± 0.04**Wh**	26	27	−0.74 ± 0.04**Wh**	22
IGN-JPL (2)	37	−1.20 ± 0.03**Wh**	**17**	33	−1.19 ± 0.17**Wh**	**14**	30	−0.94 ± 0.08**Wh**	**14**
INASAN (1)	47	−1.07 ± 0.11**Wh**	37	28	−0.91 ± 0.10**Wh**	24	25	−0.86 ± 0.08**Wh**	23
INASAN (2)	41	−1.12 ± 0.09**Wh**	**17**	33	−1.09 ± 0.17**Wh**	**15**	26	−0.88 ± 0.14**Wh**	**13**
LEGOS-CLS (1)	53	−0. 96 ± 0.05**Wh**	34	33	−0.74 ± 0. 07**Wh**	24	14	−1.04 ± 0.07**Wh**	18
LEGOS-CLS (2)	58	−1.13 ± 0.11**Wh**	**22**	28	−0.63 ± 0. 13**Wh**	**13**	15	−1.07 ± 0.12**Wh**	**10**
REUB									
IGN-JPL (1)	55	−1.16 ± 0.07**Wh**	29	24	−1.09 ± 0.10**Wh**	19	21	−0.98 ± 0.07**Wh**	17
IGN-JPL (2)	51	−0.94 ± 0.07**Wh**	**19**	28	−1.09 ± 0.07**Wh**	**14**	21	−1.37 ± 0.08**Wh**	**12**
INASAN (1)	52	−1.17 ± 0.07**Wh**	31	27	−0.94 ± 0.09**Wh**	20	21	−1.03 ± 0.07**Wh**	19
INASAN (2)	53	−1.14 ± 0.04**Wh**	**21**	27	−1.09 ± 0.04**Wh**	**15**	20	−1.28 ± 0.12**Wh**	**13**
LEGOS-CLS (1)	66	−0.80 ± 0.09**Wh**	31	20	−0.99 ± 0.06**Wh**	18	14	−0.93 ± 0.06**Wh**	15
LEGOS-CLS (2)	61	−0.91 ± 0.03**Wh**	**22**	23	−1.01 ± 0.10**Wh**	**14**	16	−0.79 ± 0.07**Wh**	**11**
REYB									
IGN-JPL (1)	44	−0.94 ± 0.13**Wh**	24	36	−0.92 ± 0.07**Wh**	21	19	−0.86 ± 0.06**Wh**	16
IGN-JPL (2)	44	−1.14 ± 0.08**Wh**	**13**	35	−0.97 ± 0.07**Wh**	**11**	21	−0.87 ± 0.08**Wh**	**8**
INASAN (1)	45	−0.78 ± 0.11**Wh**	22	35	−0.98 ± 0.07**Wh**	22	20	−0.86 ± 0.10**Wh**	15
INASAN (2)	44	−0.90 ± 0.06**Wh**	**12**	36	−0.87 ± 0. 08**Wh**	**10**	20	−1.02 ± 0.16**Wh**	**8**
LEGOS-CLS (1)	45	−1.08 ± 0.10**Wh**	20	32	−1.29 ± 0.04**Wh**	18	23	−1.10 ± 0.04**Wh**	14
LEGOS-CLS (2)	45	−0.88 ± 0.11**Wh**	**12**	29	−0.74 ± 0.11**Wh**	**9**	26	−0.92 ± 0.10**Wh**	**10**
SYPB									
IGN-JPL (1)	44	−0. 78 ± 0.21**Wh**	18	30	−0.95 ± 0.10**Wh**	17	26	−0.95 ± 0.13**Wh**	15
IGN-JPL (2)	43	−0.72 ± 0.14**Wh**	**11**	33	−1.12 ± 0.09**Wh**	**11**	23	−0.79 ± 0.10**Wh**	**9**
INASAN (1)	41	−0.82 ± 0.15**Wh**	18	32	−0.94 ± 0.12**Wh**	17	27	−0.85 ± 0.10**Wh**	15
INASAN (2)	42	−0.95 ± 0.11**Wh**	**12**	33	−0.92 ± 0.21**Wh**	**11**	24	−0.75 ± 0.08**Wh**	**9**
LEGOS-CLS (1)	42	−0.94 ± 0.05**Wh**	16	37	−0.90 ± 0.06**Wh**	15	21	−0.97 ± 0.05**Wh**	11
LEGOS-CLS (2)	39	−0.86 ± 0.06**Wh**	**9**	37	−0.58 ± 0.11**In**	**8**	25	−1.00 ± 0.06**Wh**	**8**
TLHA									
IGN-JPL (1)	51	−0.91 ± 0.08**Wh**	27	25	−0.78 ± 0.04**Wh**	20	23	−0.90 ± 0.03**Wh**	19
IGN-JPL (2)	55	−0.88 ± 0.01**Wh**	**16**	25	−0.59 ± 0.08**Wh**	**9**	19	−1.00 ± 0.15**Wh**	**9**
INASAN (1)	53	−1.10 ± 0.08**Wh**	31	26	−0.87 ± 0.06**Wh**	21	21	−0.87 ± 0.03**Wh**	19
INASAN (2)	59	−1.02 ± 0.08**Wh**	**17**	21	−0.50 ± 0.09**In**	**8**	19	−1.02 ± 0.11**Wh**	**10**
LEGOS-CLS (1)	56	−0.81 ± 0.06**Wh**	26	25	−0.69 ± 0.06**Wh**	17	20	−1.00 ± 0.06**Wh**	18
LEGOS-CLS (2)	62	−1.05 ± 0.16**Wh**	**19**	23	−0.85 ± 0.10**Wh**	**11**	15	−0.68 ± 0.11**Wh**	**8**

%Var is the percentage of explained variance, the Allan slope is given with a 1σ uncertainty. Numbers in brackets give the 90% confidence interval of the "Allan standard deviation" for a 7-day sampling time
(1) Before 2002.4, (2) after 2002.4, *Wh* white noise, *Fl* flicker noise, *In* inconclusive noise type determination

Journal: **190** MS: **88** CMS: **GIVE CMS** ☐TYPESET ☐DISK ☐LE ☐CP Disp.:**2006/8/18** Pages: **25**

(MSOB, Australia) for IGN-JPL, and Krasnoyarsk (KRAB, Russia) for LEGOS-CLS. The ASDB and MSOB series (5.2–5.7 years, depending on the ACs, and 4.1 years, respectively) are characterized by a high noise level in the height direction until 2002: the data before the availability of SPOT-5 and Envisat (i.e., before 2002) are known to be more noisier.

The ASDB series presents a jump for MSOB in the first half-year of 2004. The SPIB and SYOB time-series (4.0 and 4.2 years, respectively) are relatively short and show a shift of a few months around 2002 for SPIB and a behaviour change after 1996 for SYOB. The SAMB is an old station with less than 4 years of observations, ended in 1998 with high noise on the three components. The KRAB series (5.7 years) has a gap of 175 days and is very chaotic during the first 2 years.

Except for these few cases where the weaknesses of the time-series may explain anomalous SIs, correlation coefficients are calculated for each AC. They are 0.77, 0.52, and 0.52 for IGN-JPL, INASAN, and LEGOS-CLS, respectively. The general agreement between the two quality indices, one being based on technical geodetic expertise and the other on positioning time-series, may be considered as a reliable cross-validation of both approaches.

6.5 Latitude dependence

We noticed in Sect. 5 that some high-latitude stations have a low noise level, with inconclusive spectra. We investigate the question of a general latitude dependence using the well-observed stations (C1). In the case of GPS, Williams et al. (2004) find a noise level/latitude dependence in the GPS data. The noise level is higher in the Southern Hemisphere than in the Northern Hemisphere, probably reflecting the smaller number of baselines available for double difference data analysis, due to a sparser network distribution.

One may expect a similar effect for DORIS. Here, the amount of observations is well balanced between the Northern and Southern hemisphere, thanks to an optimal network design. Data imbalance is, however, produced by the satellite orbit inclination. The SPOT and ENVISAT satellites have polar orbits with inclinations of 98.7° and 98.55°, respectively. The TOPEX/Poseidon orbit inclination is 66.04° only. As a result, the high latitude stations are globally more observed than the others by SPOT and ENVISAT satellites and less observed by TOPEX/Poseidon (Morel and Willis 2005). However, the SPOT observations are more numerous than those by TOPEX/Poseidon, resulting in higher data rates for the high-latitude stations. Therefore, a latitude dependence of the station stability is expected to favour the polar regions.

The relationship of the SI defined in Sect.6.4 with the latitude of the stations is shown graphically in Fig. 10. The expected dependence can be seen, with the smallest values towards the poles. The zone limited by two solid lines shows the two-sigma confidence interval region of a least-squares quadratic model fit on the well-observed stations (C1). The technical ID is also plotted in Fig. 10. It shows no correlation with latitude.

Two stations with 30–40 mm outlying residuals can be pointed out. They all have relatively short observations spans that took place when only two or three satellites were available: Marion Island (MARA, South Africa) was observed over 1994.1–1998.5, Santa Maria (SAMB, Portugal Azores) was observed over 1994.1–1997.8. Apart from these special cases, the latitude dependence of station stability for the 7-day sampling time is confirmed.

7 Discussion and conclusions

Weekly time-series of positions of 119 DORIS stations in 69 sites, computed by three IDS ACs – IGN-JPL, INASAN and LEGOS-CLS – from SPOT-2, SPOT-3, SPOT-4, SPOT-5, TOPEX/Poseidon, and ENVISAT satellite observations were alnalysed. They were referred to ITRF2000 using the CATREF procedure. The data used are time-series of residuals relative to a 3D linear motion model.

The analysis method consists of applying the Allan variance spectrum identification technique to the principal components derived in the time domain (PCAT). The PCAT approach is appropriate for the study of multivariate time-series (here 3D station positions). The transformation of the signal into its time-eigenspace allows separation of independent noise contributions, thus taking into account the 3D characteristics of station motion.

On the other hand, noise characterization with the Allan variance method allows study of the signal in various time frames in one compact analysis, thus giving access to a spectral diagnosis without any a priori assumption on the type of noise. As the Allan variance method requires equally spaced data, we focussed the analysis on well observed stations (72 stations at 46 sites). The implicit assumption of the homogeneous quality of the data over the total observation span is not strictly verified in the case of DORIS, as sizeable improvement took place in 2002, with additional satellites and enhancing of the ground-beacon quality. Based on a subset of eight stations active before and after these changes, we evaluate

Journal: 190 MS: 88 CMS: GIVE CMS ☐ TYPESET ☐ DISK ☐ LE ☐ CP Disp.:2006/8/18 Pages: 25

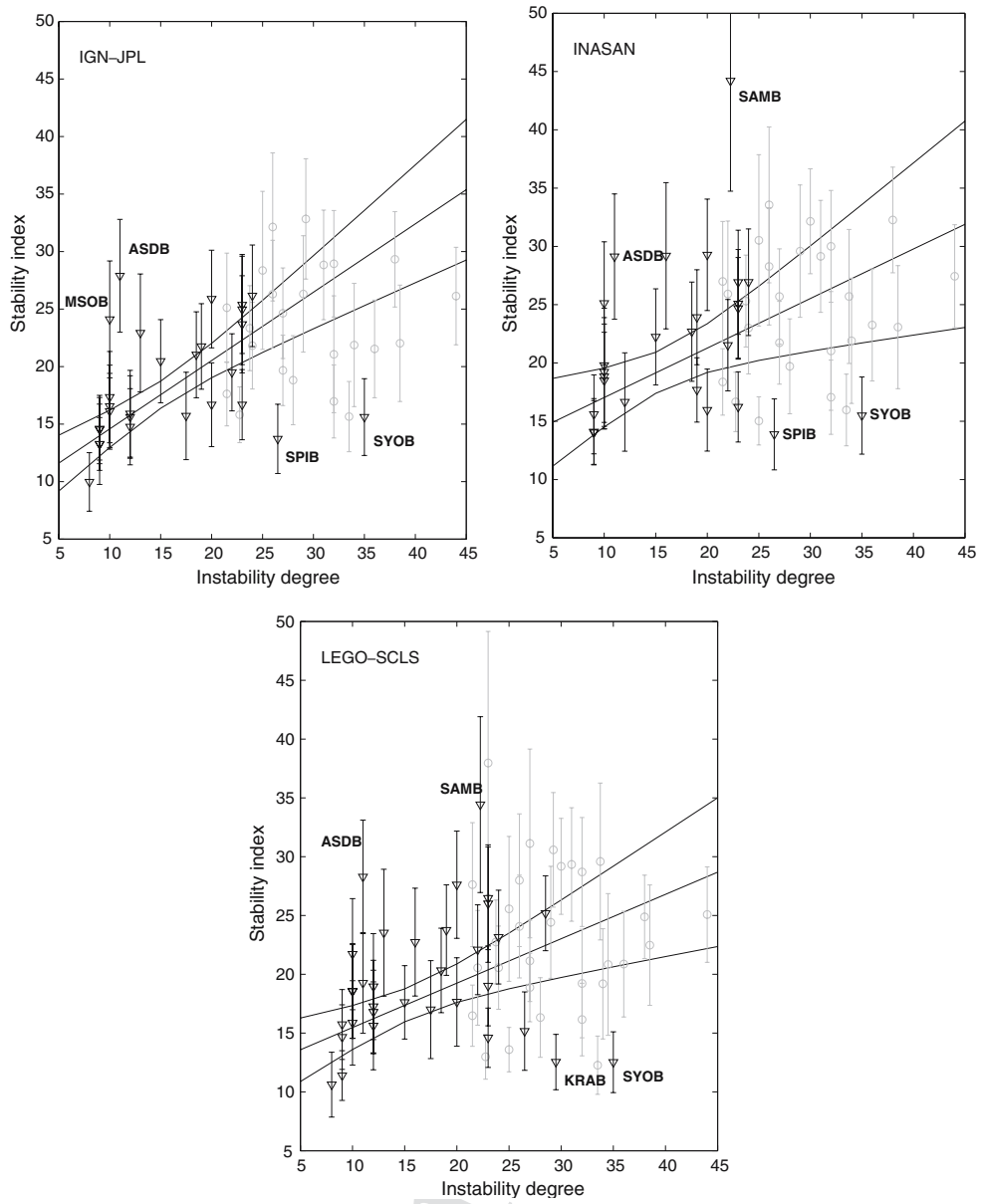

Fig. 9 Relationship between the Stability Index of DORIS stations non-linear, non-seasonal motion and the Instability Degree reflecting the station technical characteristics (Fagard 2006). The stability indices are given with a 2σ uncertainty. *Circles* Alcatel antennas, *triangles* Starec antennas. *Top left* IGN-JPL, *top right* INASAN, *bottom* LEGOS-CLS. The names of stations with outlying values are *printed*

the benefit as a decrease in short term noise by a factor of 1.3 to 2.2.

The DORIS residual time-series of station positions contains seasonal signatures or technique-specific periods such as the 117.3-day DORIS perturbation, due to aliasing of quasi-diurnal errors by the TOPEX/Poseidon orbit configuration. The amplitudes of the annual, semi-annual, and 117.3-day terms are found to reach 4.1–6.8, 2.8–4.0, and 2.9–5.5 mm respectively, considering the three ACs.

The Allan variance signature is sensitive to periodic terms. To avoid biasing the estimation of the type of noise, these three periodic terms were first filtered out by least-squares. What remains in the residual series may come from local geophysical phenomena, instrumentation, analysis strategies, or modelling errors. Their spectrum and variance level are used to qualify the station stability.

The first principal component (PC1) in the time domain of the non-linear, non-seasonal signal of the

Journal: **190** MS: **88** CMS: **GIVE CMS** ☐ TYPESET ☐ DISK ☐ LE ☐ CP Disp.:**2006/8/18** Pages: **25**

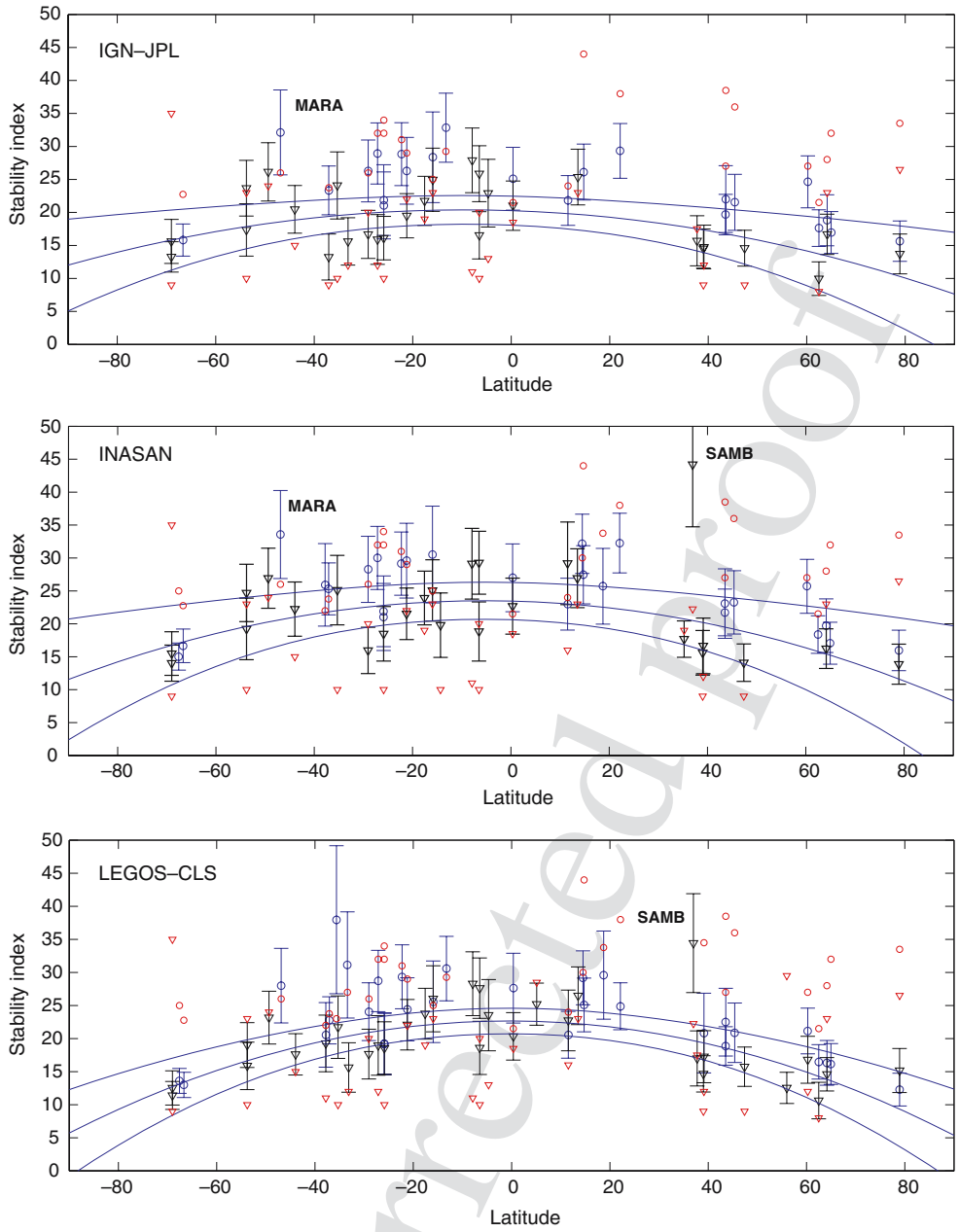

Fig. 10 Latitude dependence of the Stability Index of DORIS station coordinates. *Circles* Alcatel antennas, *triangles* Starec antennas. The stability indices are given with a 2σ uncertainty. *Top* IGN-JPL, *middle* INASAN, *bottom* LEGOS-CLS

DORIS time-series represents 40–60% of the total signal and shows 10–45 mm white noise; then, the second component at a level of 20–40% has 10–40 mm white noise, and the remaining component is 10–28 mm white noise explaining 17–30% of the signal.

Most of the DORIS satellites have high inclinations, resulting in roughly North–South orientation of the satellite passes over the stations. This pass geometry implies a poor determination of the East station coordinates. This is confirmed by our results, which show that the first PCAT is highly correlated with the East direction for most stations and all ACs. The "Allan standard deviation" is the largest in the East direction. The noise levels in the North and height directions are 10–30 mm.

Stations at high latitude are tracked by the SPOT and ENVISAT satellites only. Because of the orbit configuration of these satellites, the number of observations is larger than for the other stations. Their short-term

Journal: 190 MS: 88 CMS: GIVE CMS ☐ TYPESET ☐ DISK ☐ LE ☐ CP Disp.:2006/8/18 Pages: 25

stability is better than the average, at the 15–20 mm level. Their noise type determination is poor, the estimator of the Allan graph value being close to the virtual border between white and flicker noise.

A couple of case studies of our approach show that the inspection of time-series in their time-eigenspace permits one to isolate signatures that cannot be seen otherwise. The analysis of HBKB (Hartebeesthoek, Africa) points to an additional perturbation that is still unmodelled in the DORIS analysis, as the increasing number of observation satellites in 2002.4 does not improve the noise in the East direction as it does in the other two directions. A second aspect concerns the second privileged direction: it is different for IGN-JPL/INASAN and LEGOS-CLS, probably due to differences in the software and the analysis strategies that might deserve further investigation.

Maximum likelihood estimation is often used in geodetic time-series analysis to estimate their type and level of noise. It is based on the rigorous definition of a model for each time-series, including an ad hoc analytical model for the signal (e.g. drift, constant bias, and periodic terms) and a stochastic model for the noise. The analysis consists in determining, for each time-series, the parameters of the model and testing the validity of the assumptions. This method is insensitive to irregular data intervals and gaps, and is thus appropriate for positioning data.

The Allan variance analysis requires regular data intervals, which is – in principle – the situation of satellite-geodetic time-series of positions. However, data gaps can be filled by a technique transparent to the analysis for well-observed stations. Meanwhile, it is free of any a priori assumption and the type of noise determination is rapid and direct, through the interpretation of the Allan graph controlled by a Fisher test.

Another difference of the method used here is the fact that PCAT takes into account the 3D motion of the stations, while the MLE implementation found in the literature treats the motion in the three local directions sequentially. Finally, the MLE result consists of a mix of noises for each time-series, whereas the coupled PCAT–Allan variance method concludes on one type of noise for each direction in the time-eigenspace, which can then be reconnected to the local frame directions. It is hoped that the advantages and drawbacks of these two approaches will be further discussed in the future.

Acknowledgements The three DORIS solutions analysed here were referred to ITRF2000 by Jean-Jacques Valette (IDS Central Bureau) using the CATREF software. I thank him for providing the residual time-series and for discussing, in detail, some of my results. I thank Will Featherstone, Thomas Herring, Burkhard Schaffrin, Simon Williams, Pascal Willis and an anonymous reviewer who provided helpful review comments.

References

Allan DW (1966) Statistics of atomic frequency standards. IEEE Trans 54:221–231

Allan DW (1987) Time and frequency (time-domain) characterization, estimation, and prediction of precision clocks and oscillators. IEEE Trans 34:647–654

Altamimi Z, Sillard P, Boucher C (2002) ITRF2000: a new release of the International Terrestrial Reference Frame for earth science applications. J Geophys Res 107(B10):2214. DOI 10.1029/2001JB000561

Azoubib J (1974) Caractérisation des fluctuations aléatoires d'un processus temporel par la variance d'Allan. Report 74/7. Bureau International des Poids et Mesures (BIPM), Sèvres

Baccini A, Besse P (1999) Statistique descriptive multidimensionnelle. In: Laboratoire de Statistique et Probabilité publications. Paul Sabatier University, Toulouse

Beutler G, Rothacher M, Schaer S, Springer TA, Kouba J, Neilan RE (1999) The international GPS service (IGS): an interdisciplinary service in support of Earth sciences. Adv Space Res 23(4):631–653. DOI 10.1016/S0273-1177(99)00160-X

Blewitt G, Lavallée D (2002) Effect of annual signals on geodetic velocity. J Geophys Res 107(B7):2145. DOI 10.1029/2001JB000570

Crétaux JF, Soudarin L, Davidson F JM, Gennero MC, Berge-Nguyen M, Cazenave A (2002) Seasonal and interannual geocenter motion from SLR and DORIS measurements: comparison with surface loading data. J Geophys Res 107(B12):2374. DOI 10.1029/2002JB001820

Fagard H (2006) Twenty years of evolution of the DORIS network: from its initial deployment to its renovation. J Geod (in press, same issue)

Feissel-Vernier M, Le Bail K (2006) Spectral characteristics of the measurement of station motion with GPS. In: Gowey K (ed) IGS Technical Report 2003/04. IGS Central Bureau, Jet Propulsion Laboratory, Pasadena (in press)

Greenhall CA (1991) Recipies for degrees of freedom of frequency stability estimators. IEEE Trans Instrum Meas 40(6):994–999

Howe DA, Allan DW, Barnes JA (1981) Properties of signal sources and measurement methods. In: Proceedings of IEEE 35th annual symposium on frequency control, 27–29 May 1981, pp A1–A47

Hugentobler U, Dach R, Meindl M, Fridez P (2005) Bernese GPS Software Version 5.0. Astronomical Institute University of Berne, Berne

Hugentobler U, Meindl M, Beutler G, Bock H, Dach R, Jäggi A, Urschl C, Mervart L, Rothacher M, Schaer S, Brockmann E, Ineichen D, Wiget A, Wild U, Weber G, Habrich H, Boucher C (2006) CODE IGS Analysis Center Technical Report 2003/04. In: Gowey K (ed) IGS Technical Report 2003/04. IGS Central Bureau, Jet Propulsion Laboratory, Pasadena (in press)

King NE, Svarc JL, Fogleman EB, Gross WK, Clark KW, Hamilton GD, Stiffler CH, Sutton JM (1995) Continuous GPS observations across the Hayward fault, California, 1991–1994. J Geophys Res 100(B10):20271–20284. DOI 10.1029/95JB02035

Kuzin SP, Tatevian SK (2006) Determination of seasonal geocenter variations from DORIS, GPS and SLR data. In: Capitaine (ed) Earth dynamics and reference systems: five years after adoption of the IAU 2000 Resolutions. Proc Journées Systèmes de Référence spatio-temporels (in press)

Langbein JO, Johnson H (1997) Correlated errors in geodetic time series: Implications for time-dependent deformation. J Geophys Res 102(B1):591–603. DOI 10.1029/96JB02945

Le Bail K (2004) Etude statistique de la stabilité des stations de géodésie spatiale. Applicationà DORIS. 10 Dec 2004. PhD Thesis dissertation in "Dynamique des systèmes gravitationels", Paris Observatory

Le Bail K, Valette JJ, Zerhouni W, Feissel-Vernier M (2006) Long-term consistency of multi-technique terrestrial reference frames, a spectral approach. In: Tregoning P, Rizos C (eds) Monitoring and Understanding a Dynamic Planet with Geodetic and Oceanographic Tools. Springer, Berlin Heidelberg New York (in press)

Lemoine J-M, Capdeville H Corrective model for Jason-1 DORIS Doppler data in relation to the South Atlantic Anomaly. J Geod (same issue, in press)

Mao A, Harrison CGA, Dixon TH (1999) Noise in GPS coordinate time series. J Geophys Res 104(B2):2797–2816. DOI 10.1029/1998JB900033

Morel L, Willis P (2005) Terrestrial reference frame effects on global sea level rise determination from TOPEX/Poséidon altimetric data. Adv Space Res 36(3):358–368. DOI 10.1016/j.asr.2005.05.113

Nikolaidis R (2002) Observation of geodetic and seismic deformation with the Global Positioning System. PhD Thesis dissertation, University of California in San Diego

Papoulis A, Pillai SU (2002) In: International edition. Probability, random variables and stochastic processes, 4th edn. McGraw-Hill, New York, pp 249–250

Pavlis DE, Poulose SG, Rowton SC, McCarthy JJ, Luthcke SB (2000) GEODYN operations manuals. Contractor report Raytheon ITSS, Greenbelt, 15 March 2000

Pearlman MR, Degnan JJ, Bosworth JM (2002) The international laser ranging service. Adv Space Res 30(2):135–143. DOI 10.1016/S0273-1177(02)00277-6

Penna NT, Stewart MP (2003) Aliased tidal signatures in continuous GPS height time series. Geophys Res Lett 30(23):2184–2187. DOI 10.1029/2003GL018828

Rutman J (1978) Characterization of phase and frequency instabilities in precision frequency sources: fifteen years of progress. Proc IEEE 66:1048–1075

Saporta G (1978) In: TECHNIP (ed) Théories et Méthodes de la Statistique. Institut Français du Pétrole publications, Paris.

Schlueter W, Himwich E, Nothnagel A, Vandenberg N, Whitney A (2002) IVS and its important role in the maintenance of the global reference systems. Adv Space Res 30(2):145–150. DOI 10.1016/S0273-1177(02)00278-8

Sillard P, Boucher C (2001) A review of algebraic constraints in Terrestrial Reference Frame datum definition. J Geod 75(2-3):63–73. DOI 10.1007/s001900100166

Snajdrova K, Boehm J, Willis P, Haas R, Schuh H (2006) Multi-technique comparison of tropospheric zenith delays derived during the CONT02 campaign. J Geod 79(10-11):613–623. DOI 10.1007/s00190-005-0010-z

Soudarin L, Crétaux JF (2006) A model of present-day tectonic plate motions from 12 years of DORIS measurements. J Geod (same issue, in press)

Tavernier G, Fagard H, Feissel-Vernier M, Lemoine F, Noll C, Ries J, Soudarin L, Willis P (2005) The International DORIS Service (IDS). Adv Space Res 36(3):333–341. DOI 10.1016/j.asr.2005.03.102

Tavernier G, Fagard H, Feissel-Vernier M, Le Bail K, Lemoine F, Noll C, Ries J, Soudarin L, Valette JJ, Willlis P (2006) The International DORIS Service: genesis and early achievements. J Geod (same issue, in press)

Webb FH, Zumberge JF (1997) An introduction to GIPSY-OASIS II: precision software for the analysis of data from the Global Positioning System, Internal Publication JPL D-11088. Jet Propulsion Laboratory, Pasadena

Williams SDP (2003) The effect of coloured noise on the uncertainties of rates estimated from geodetic time series. J Geod 76(9-10):483–494. DOI 10.1007/s00190-002-0283-4

Williams SDP, Bock Y, Fang P, Jamason P, Nikolaidis RM, Prawirodirdjo L, Miller M, Johnson DJ (2004) Error analysis of continuous GPS position time series. J Geophys Res 109(B3):B03412. DOI 10.1029/2003JB002741

Williams SDP, Lavallée DA, Penna N (2005) The effect of discontinuities, noise and geophysical signals on the maintenance of a Terrestrial Reference Frame. EOS Trans AGU 86(52), Fall Meet. Suppl., Abstract G32A-02

Willis P, Heflin MB (2004) External validation of the GRACE GGM01C gravity field using GPS and DORIS positioning results. Geophys Res Lett 31(13):L13616. DOI 10.1029/2004GL020038

Willis P, Haines B, Berthias JP, Sengenes P, Le Mouel JL (2004) Comportement de l'oscillateur DORIS/Jason au passage de l'anomalie sud-atlantique, Behavior of the DORIS/JASON oscillator over the South Atlantic Anomaly. CR Geoscience 336(9):839–846. DOI 10.1016/j.crte.2004.01.004.

Willis P, Lemoine FG, Soudarin L (2005) Looking for systematic error in scale from terrestrial reference frames derived from DORIS data. In: Tregoning P, Rizos C (eds) Monitoring and Understanding a Dynamic Planet with Geodetic and Oceanographic Tools. Springer, Berlin Heidelberg New York (in press)

Willis P, Ries JC (2005) Defining a DORIS core network for Jason-1 precise orbit determination based on ITRF2000: methods and realization. J Geod 79(6-7):370–378. DOI 10.1007/s00190-005-0475-9

Willis P, Berthias JP, Bar-Sever YE (2006) Systematic error in the Z-geocenter derived using satellite tracking data: a case study from SPOT-4 DORIS data in 1998. J Geod 79(10–11):567–572. DOI 10.1007/s00190-005-0013-9

Zhang J, Bock Y, Johnson H, Fang P, Genrich JF, Williams S, Wdowinski S, Behr J (1997) Southern California Permanent GPS Geodetic Array: error analysis of daily position estimates and site velocities. J Geophys Res 102(B8):18035–18055. DOI 10.1029/97JB01380